

Influence of the Last Glacial Maximum on New Jersey shelf offshore fresh groundwater reservoirs - investigating the role of geological heterogeneity

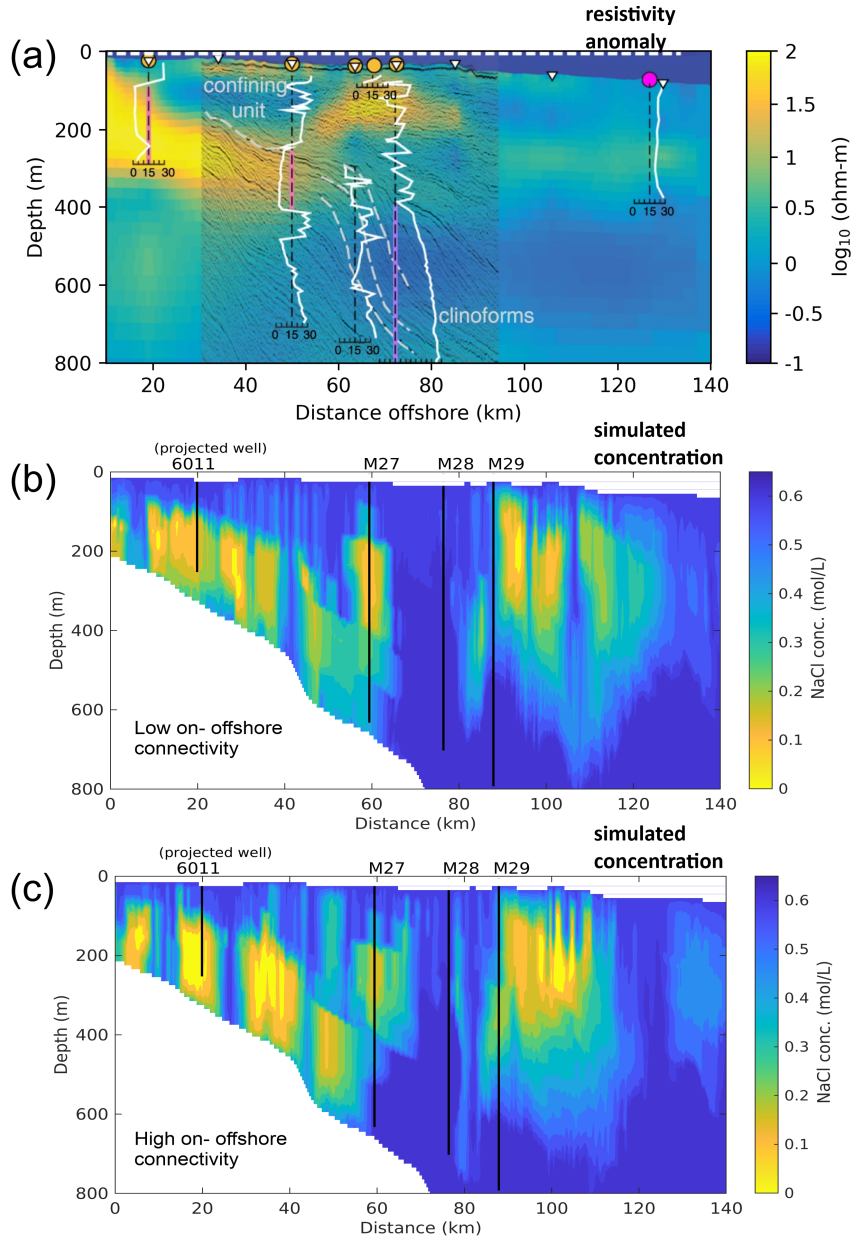
Ariel T Thomas¹, Sönke Reiche¹, and Christoph Clauser¹

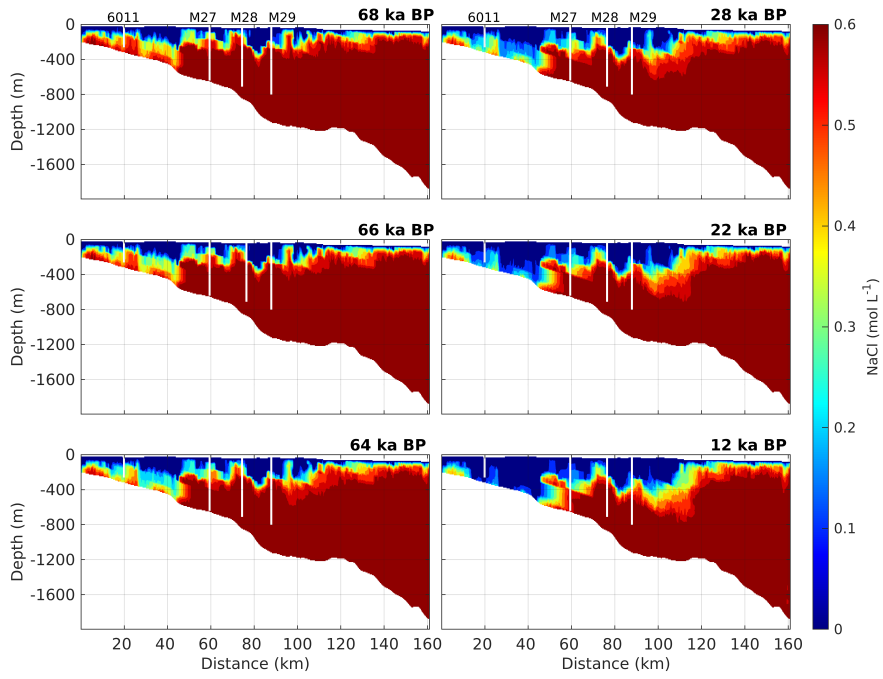
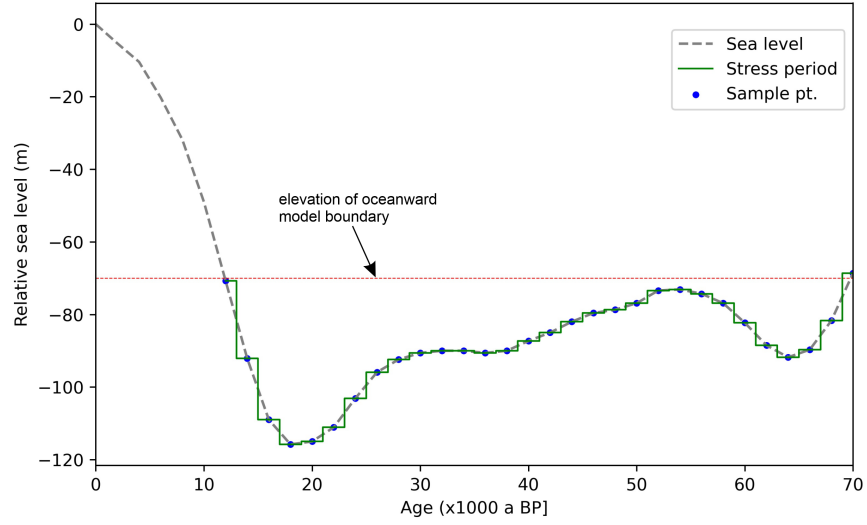
¹RWTH Aachen University

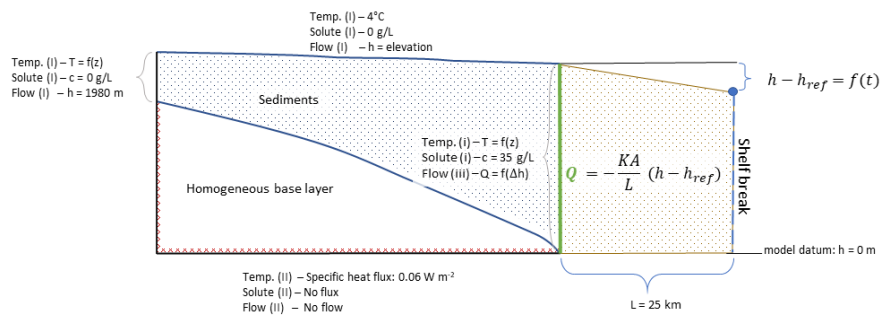
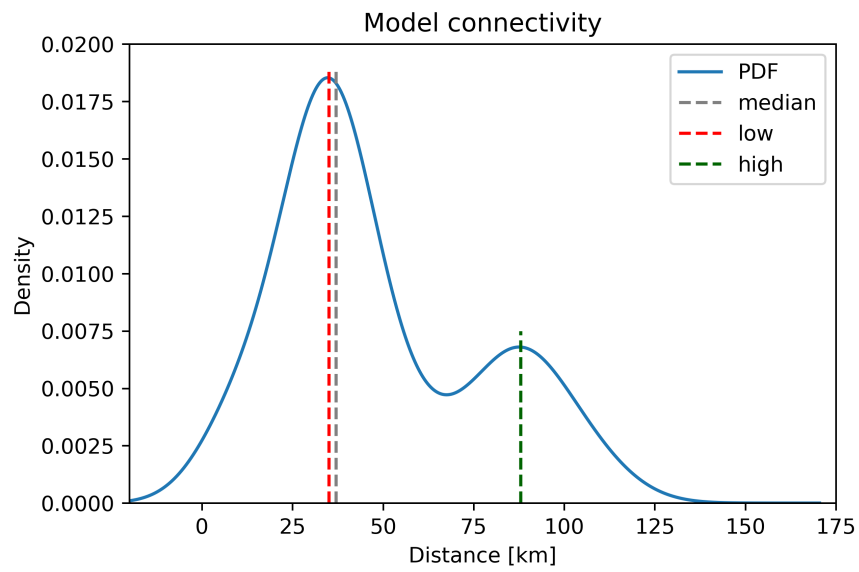
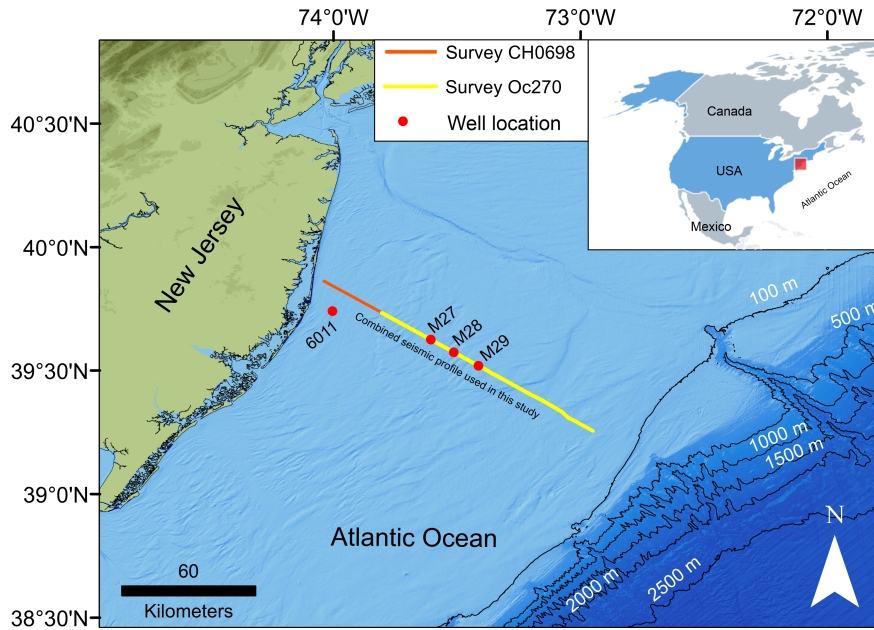
November 23, 2022

Abstract

Offshore freshened groundwater reservoirs occur on continental shelves in several regions of the world. Their origins are an active area of research, however, models often rely on simplified geometrical representations of subsurface geology. The New Jersey shelf hosts an extensive multi-layered freshened groundwater system that previous paleo-reconstructions have not reproduced. In this numerical case-study, we aim to characterize the New Jersey shelf system in the context of a geologically representative heterogeneous model. Our model combines sequence stratigraphic interpretation of 2D depth migrated seismic lines and a stochastic facies distribution with petrophysical properties of four boreholes. We employ a stochastic approach to generate both high and low onshore-offshore connectivity scenarios. The study considers a 58 000-year recharge period for the subaerially exposed shelf transect, followed by the marine transgression from 12 000 years ago until today. The results show that the lowstand period drove sufficient freshwater emplacement that can explain most of the present-day observations. The highest rates of recharge occurred during the periods of most rapid sea-level fall. Simulated scenarios indicate that topographically driven flow of meteoric recharge via surface-connected pathways is the key emplacement mechanism. Surviving freshwater systems exhibit lateral variability in salinity due to downward fingering of saline pore fluid. Freshwater preserved from the Last Glacial Maximum may extend up to 100 km from the coastline. The results also suggest that cyclical flushing and re-salinization of shelf sediments during glacial-interglacial cycles is an asymmetrical process, promoting freshwater storage over geological time scales.







1 **Influence of the Last Glacial Maximum on New Jersey**
2 **shelf offshore fresh groundwater reservoirs – investigating**
3 **the role of geological heterogeneity**

4 **Ariel T. Thomas¹, Sönke Reiche¹, Christoph Clauser¹**

5 ¹Institute for Applied Geophysics and Geothermal Energy, RWTH Aachen University,
6 Mathieustrasse 30, 52074 Aachen, Germany.

7

8 Corresponding author: Ariel T. Thomas (athomas@eonerc.rwth-aachen.de)

9 **Key Points:**

- 10 • The Pleistocene sealevel lowstand provided sufficient conditions to freshen most of the
11 mid-Miocene sediments on the New Jersey shelf.
- 12 • Onshore-offshore connectivity is not required to explain the mid-shelf freshened
13 reservoirs.
- 14 • Downward fingering of saltwater via seafloor-connected pathways in the sediment column
15 compartmentalizes the preserved freshwater system.

16 **Abstract**

17 Offshore freshened groundwater reservoirs occur on continental shelves in several regions of the
18 world. Their origins are an active area of research, however, models often rely on simplified
19 geometrical representations of subsurface geology. The New Jersey shelf hosts an extensive multi-
20 layered freshened groundwater system that previous paleo-reconstructions have not reproduced.
21 In this numerical case-study, we aim to characterize the New Jersey shelf system in the context of
22 a geologically representative heterogeneous model. Our model combines sequence stratigraphic
23 interpretation of 2D depth migrated seismic lines and a stochastic facies distribution with
24 petrophysical properties of four boreholes. We employ a stochastic approach to generate both high
25 and low onshore-offshore connectivity scenarios. The study considers a 58 000-year recharge
26 period for the subaerially exposed shelf transect, followed by the marine transgression from 12
27 000 years ago until today. The results show that the lowstand period drove sufficient freshwater
28 emplacement that can explain most of the present-day observations. The highest rates of recharge
29 occurred during the periods of most rapid sea-level fall. Simulated scenarios indicate that
30 topographically driven flow of meteoric recharge via surface-connected pathways is the key
31 emplacement mechanism. Surviving freshwater systems exhibit lateral variability in salinity due
32 to downward fingering of saline pore fluid. Freshwater preserved from the Last Glacial Maximum
33 may extend up to 100 km from the coastline. The results also suggest that cyclical flushing and re-
34 salinization of shelf sediments during glacial – interglacial cycles is an asymmetrical process,
35 promoting freshwater storage over geological time scales.

36

37

38

39

40

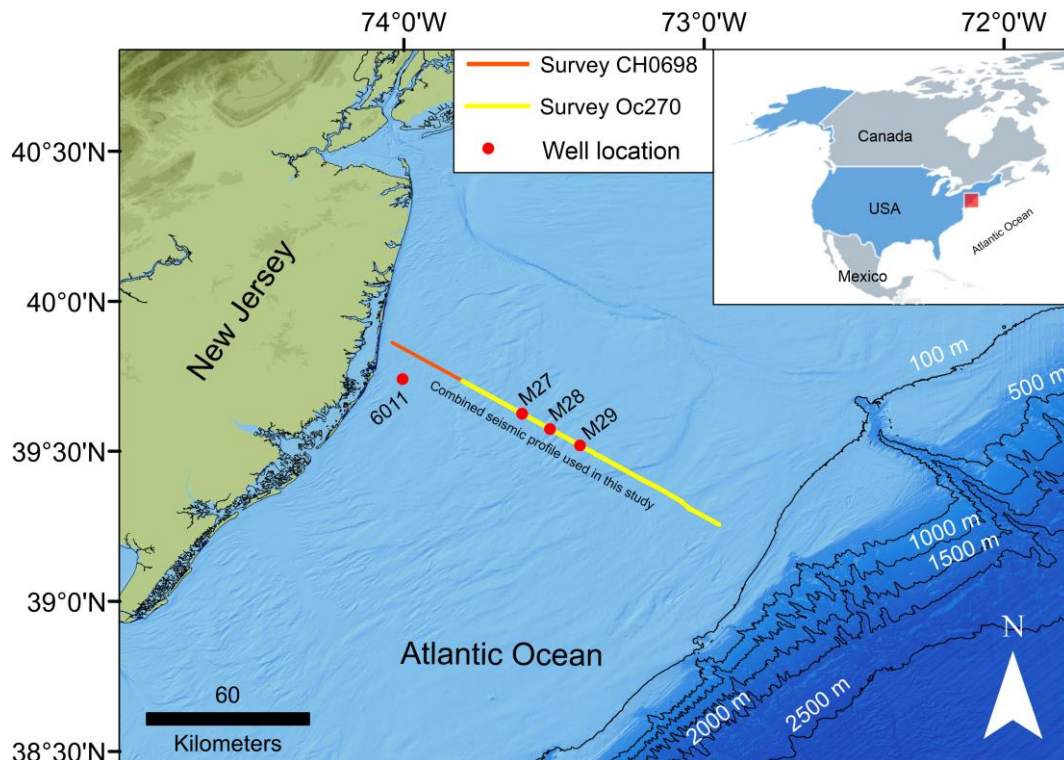
41

42

43 Plain Language Summary

44 Large volumes of freshwater have been found in sediments on continental margins worldwide.
 45 On-going research aims to explain their origins and potential resource viability. The area offshore
 46 New Jersey on the Central Atlantic coast of North America contains a complex freshwater
 47 reservoir system. We conducted simulations incorporating the existing field data to analyze the
 48 history of fluids in the subsurface from the last ice-age until today. Over this period, relatively low
 49 sea-level allowed previously salty regions of the subsurface to become flushed with freshwater.
 50 We examine the factors which influence the speed and extent of this process. The results show that
 51 large volumes of freshwater entered the subsurface at distances over 100 km from the current
 52 coastline. As the planet warmed and sealevel rose, complex layering of the rocks in the subsurface
 53 protected a portion of this freshwater from the salty ocean water. These offshore reservoirs may
 54 contain significant amounts of fresh groundwater and we need to improve our understanding of
 55 these complex systems.

56 1 Introduction



57
 58 *Figure 1 Study location map showing composite seismic line and location of IODP Expedition 313 wells and AMCOR site 6011.*

59 The existence of large reserves of fresh to brackish water in continental shelf sediments has been
60 identified as a global phenomenon (Post et al. 2013). Several studies have investigated these
61 dynamic systems in a number of settings (Groen et al. 2000; Johnston 1983; Lofi et al. 2013;
62 Micallef et al. 2020b), leading to an increased understanding of the key factors that influence the
63 emplacement and survival of offshore fresh groundwater (OFG). A study by Meisler et al. (1984)
64 identified eustatic sea-level changes as a key driver of freshwater emplacement in the New Jersey
65 shelf. Periods of relative sea-level lowstand results in increased hydraulic gradients, driving more
66 freshwater offshore. The sub-aerial exposure of shelf sediments allows for surface recharge by
67 meteoric water. Kooi et al. (2000) performed a numerical study on theoretical shelf models that
68 examined the variety of ways in which emplaced freshwater can be preserved in shelf sediments.
69 The results showed preservation to be a function of the rate of marine transgression as well as the
70 aquifer geometries in the substrate. Glacial – interglacial cycles are known to cause significant
71 sea-level variations and therefore, are fundamentally intertwined with the lifecycle of offshore
72 fresh groundwater. The impact of the Pleistocene glaciation has been examined in regional scale
73 numerical studies on the North American Atlantic margin (Cohen et al. 2010; Siegel et al. 2014).
74 These studies found that the presence of ice-sheet cover contributed significantly to offshore fresh
75 groundwater volumes. It led to increased recharge by subglacial meltwater, and enhanced offshore
76 hydraulic heads due to glacial loading.

77 The New Jersey shelf sits on the US mid-Atlantic margin, and is considered a classic passive
78 margin setting, with no significant tectonic controls on the sediments. The sedimentary record
79 shows that by the early Oligocene a major shift had occurred from a carbonate ramp deposition to
80 predominantly siliclastic sedimentation (Miller and Snyder 1997). These sediments have been
81 explored by several scientific drilling campaigns. The Atlantic Margin Coring Project (AMCOR)
82 was conducted by the U.S. Geological Survey in 1976. Hathaway et al. (1979) reported that pore
83 fluid studies revealed that much of the Atlantic continental shelf contains fresh – brackish
84 groundwater. Subsequent campaigns include the Ocean Drilling Program legs 150, 150X, 174 and
85 174X (Austin et al. 1998; Miller et al. 1994); and most recently the International Ocean Discovery
86 Program (IODP) Expedition 313 (Mountain et al. 2010). These later studies were designed to
87 investigate the link between Cenozoic sea-level change and the sedimentary record at the New
88 Jersey shelf. However, pore fluid analysis of core samples by Mountain et al. (2010) revealed
89 multiple layers of fresh – brackish groundwater in the mid-shelf region. The freshwater reservoirs

90 occur primarily in late Oligocene – Miocene sediments, with low-salinity intervals encountered at
91 depths ranging from just below the seafloor down to 500 m.

92 Since the initial discovery of extensive offshore freshened groundwater reserves during the
93 AMCOR drilling project (Hathaway et al. 1979), there have been several studies aimed at
94 understanding the hydrogeological evolution of these reservoirs. It was first assumed that the
95 freshwater body was a homogeneous, flat-lying plume, which extended oceanward becoming
96 gradually thinner and more saline. The lens was thought to be fed by submarine groundwater
97 discharge derived from the terrestrial domain. Meisler et al. (1984) conducted a series of
98 simulations on a simple, layered geological model of New Jersey shelf. The study investigated the
99 impact of sea-level, hydraulic conductivity and various permeability anisotropy ratios on the
100 position of a sharp freshwater – seawater interface. Meisler et al. (1984) concluded that the position
101 of the interface was not in equilibrium with present-day sea-level. The authors speculated that
102 freshwater could have been emplaced as early as the Miocene period. Pope and Gordon (1999)
103 investigated the position of the interface on the New Jersey shelf in numerical simulations,
104 implementing sea level variations over a period of 84 000 years. The authors concluded that due
105 to enhanced recharge and discharge of freshwater driven by a fall in sea-level, the oceanward
106 migration of the interface occurs more rapidly relative to the slow-moving rebound when sea-level
107 rises.

108 A later study analyzing oxygen isotope data by Malone et al. (2002) found that the offshore low-
109 salinity plume was not homogenous, as previously assumed. Oxygen isotope analysis of samples
110 collected in Ocean Drilling Project Leg 174a (Austin et al. 1998) revealed the internal structure of
111 the freshwater distribution in the upper 400 m of the sediment column. The variation was then
112 assumed to be related to high-porosity sand-rich intervals. Pore fluid analysis performed as part of
113 IODP Expedition 313 (sites M27, M28 and M29) revealed a multi-layered reservoir system, with
114 sharp boundaries between fresh and overlying salt water intervals (Mountain et al. 2010). Detailed
115 core analysis by Lofi et al. (2013) revealed that freshwater occurred preferentially in low-
116 permeability intervals, contrary to earlier assumptions. However, this correlation was not
117 ubiquitous. Lofi et al. (2013) presented a new hydrogeological conceptual model of the New Jersey
118 shelf that consisted of multi-layered freshwater reservoirs of varying thickness. Lofi et al. (2013)
119 also suggested that there may be multiple mechanisms of freshwater emplacement responsible for

120 present day observations. The absolute ages of pore fluid samples from IODP Expedition 313 have
121 not been determined, so the time since these samples have been buried is uncertain. A study by
122 van Geldern et al. (2013) used stable isotope geochemical analysis to argue for a modern meteoric
123 origin of the freshwater. However, the possibility of paleo-groundwater recharge in a period with
124 isotope levels similar to present-day could not be ruled out. Regional numerical studies by Cohen
125 et al. (2010) and Person et al. (2003) identify meteoric recharge during Pleistocene sea-level
126 lowstand as the key source of the freshwater. A resistivity model presented by Gustafson et al.
127 (2019) shows a high-resistivity anomaly, attributed to low salinity pore fluid, which extends
128 landward of the IODP Expedition 313 sites. The authors conclude that the anomaly, obtained by
129 jointly inverting surface-towed controlled source electromagnetic and sea-floor magnetotelluric
130 data, is consistent with land-derived recharge of the offshore freshwater reservoirs.

131 Research on the origins of the freshwater on the New Jersey shelf has therefore converged around
132 two hypotheses: (1) Fresh groundwater was emplaced during Pleistocene glacial periods, where
133 large parts of the shelf were subaerially exposed. Sea-level lowstand resulted in an increase in the
134 hydraulic head gradient, driving vigorous groundwater flow towards the open sea (Cohen et al.
135 2010; Hathaway et al. 1979; Person et al. 2003), (2) Offshore fresh groundwater reservoirs are
136 hydraulically connected with onshore aquifers, implying modern recharge by seaward-flowing
137 meteoric groundwater (Gustafson et al. 2019; van Geldern et al. 2013). To date, no study has been
138 conducted on New Jersey samples to determine absolute ages of the freshwater. Previous regional
139 studies did not aim to capture the geological heterogeneity and therefore could not conclusively
140 explain the observed layered distribution. Advances in computing capability have enabled more
141 rigorous testing of larger and increasingly complex hydrogeological models on the Atlantic margin
142 (Cohen et al. 2010; Siegel et al. 2014; Thomas et al. 2019). This has expanded the understanding
143 of mechanisms driving freshwater emplacement and subsequent survival.

144 The primary focus of this study is to use a geologically heterogeneous shelf model to test the
145 hypothesis that fresh groundwater was emplaced in New Jersey shelf sediments during the period
146 of extended sea-level lowstand associated with the Last Glacial Maximum (LGM). We conducted
147 coupled variable-density flow and heat transport simulations on the 2D shelf transect shown in
148 Figure 1. The shelf model was generated using a workflow originally presented in Thomas et al.
149 (2019). We used a stochastic modelling approach known as Sequential Indicator Simulation (SIS)

150 to determine a facies distribution, constrained by 2D depth migrated seismic and well data.
151 Porosity and permeability values are assigned to the model domain based on the facies. This
152 approach produces a geologically representative model that captures key characteristics of the
153 sediment heterogeneity and therefore accounts for its influence on the observed salinity
154 distribution. We use a process-based criterion to assess the distribution of flow connectivity in a
155 suite of 100 model realizations. We then selected the two models representing the high- and low
156 onshore-offshore connectivity cases.

157 We simulated paleo-hydrogeological conditions on the New Jersey transect during the period from
158 the LGM to present day. We consider the past 70 000 years of the hydrogeological evolution of
159 the New Jersey shelf. Firstly, simulations were performed to investigate the sensitivity of the
160 model to key factors that influence offshore freshened groundwater on the continental shelf: (1)
161 topographically driven flow (base case), (2) cemented intervals, (3) enhanced terrestrial discharge
162 and (4) permeability anisotropy. In order to model a meteoric recharge scenario, we consider the
163 specific period of the Pleistocene when the entire surface of the modelled transect was sub-aerially
164 exposed. We determined this recharge phase to be from 70 000 to 12 000 years before present
165 (BP), based on the seafloor bathymetry (Ryan et al. 2009) and sea-level data (Imbrie et al. 1984).
166 The influence of the four factors on the dynamics and distribution of fresh groundwater
167 emplacement on the New Jersey shelf was quantified by comparing the relative volumes of
168 emplaced freshwater at the end of the recharge phase, and at present day. Finally, we simulated
169 the lowstand period considering combinations of the aforementioned driving factors, as plausible
170 reconstructions of hydrogeological scenarios over the past 70 000 years. These simulations allow
171 us to draw conclusions about the evolution of offshore freshened groundwater reservoirs observed
172 in IODP Expedition 313.

173 We conducted this analysis on a detailed hydrogeological model in order to account for the role of
174 geological heterogeneity in the complex distribution presently observed. These simulations aim to
175 deduce whether meteoric recharge of freshwater on the New Jersey shelf during the last glacial
176 maximum could sufficiently explain present-day observations given a plausible reconstruction of
177 paleo-conditions.

178 **2 Methodology**

179 **2.1 Seismic interpretation to hydrogeological model**

180 Modelling paleo-groundwater flow on the New Jersey shelf poses the challenge of characterizing
181 the distribution of petrophysical properties in a domain with limited well control. In this study, we
182 generate a facies distribution model utilizing the workflow originally presented in detail by
183 Thomas et al. (2019). The approach combines seismic interpretation with well log analysis to
184 constrain a sequential indicator simulation algorithm. The seismic interpretation presented in
185 Thomas et al. (2019) was extended to include the most landward extensions of the sequences that
186 have been imaged by seismic data. Depth migrated 2D seismic lines are used to constrain the
187 sequence stratigraphic boundaries (Riedel et al. 2018). The profiles include CH068-19 (R/V Cape
188 Hatteras expedition 0698) and OC 270 lines 529, 129-429 and 29 (R/V Oceanus expedition
189 OC270). The nomenclature for the interpreted Miocene sequences were defined after Miller et al.
190 (2013). The extended interpretation is shown in Figure 2.

191 The model domain is centered on adjacent 2D seismic lines which extend 161 km from the coast
192 to close to the shelf edge. The interpretation shown in Figure 2 consists of 25 horizons, from the
193 ocean floor to the lowermost sequence boundary o1, identified as the Eocene-Oligocene boundary
194 (Miller et al. 2013). This basal sequence is the deepest horizon for which a coherent seismic event
195 could be identified. Below this surface, homogeneous model properties were assigned. The 2D
196 model domain has dimensions of 161 km x 2 km and is discretized on a finite difference grid. Cell
197 dimensions are constant throughout the model domain at 100 m in the horizontal and 10 m in the
198 vertical. The entire model comprises 322 000 cells.

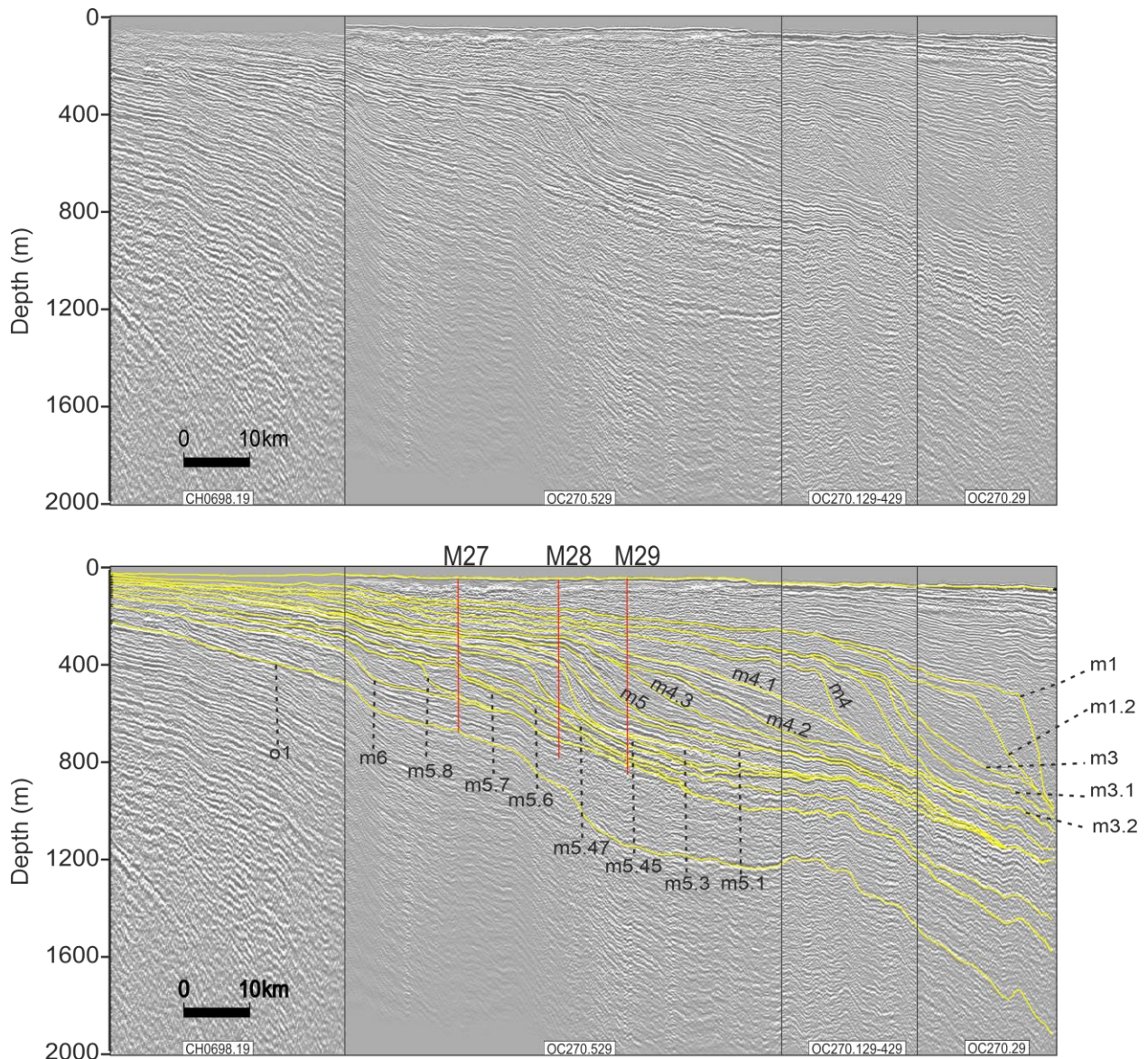


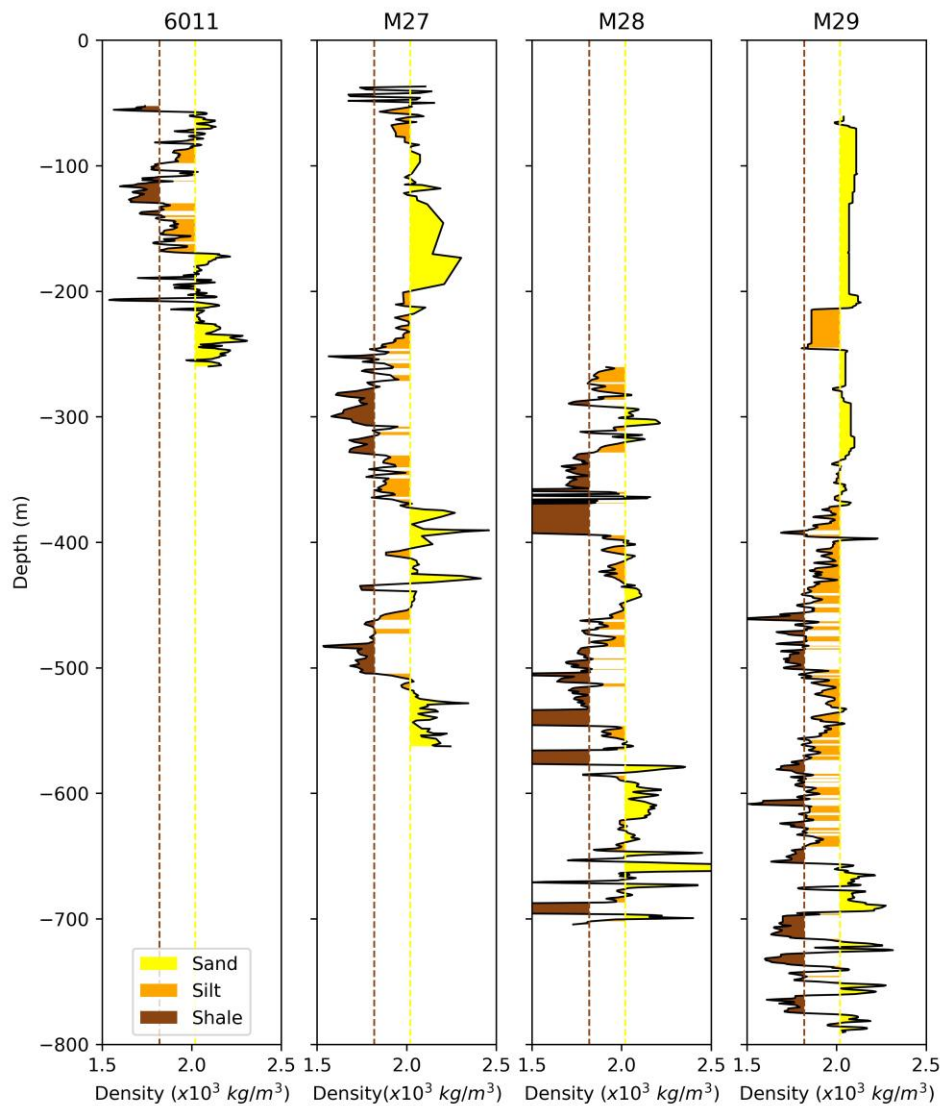
Figure 2 Seismic interpretation of New Jersey shelf sequences on adjacent 2D depth migrated lines CH0698.19, OC270.529, OC270.129-429, OC270.29

199
200
201

202 The stratigraphic framework, shown in Figure 2 was characterized with a facies distribution using
 203 Sequential Indicator Simulations (SIS). This stochastic approach is a variogram-based simulation
 204 of categorical variables, which can be constrained by well data as well as quantified geological
 205 trends (Deutsch and Pyrcz 2014). In our implementation of the SIS algorithm, stochastic
 206 realizations are constrained by estimated vertical and horizontal correlation lengths, seismic
 207 reflector orientation, as well as vertical and horizontal probability trends derived from interpreted
 208 well log data.

209 Well data of IODP expedition 313 (Mountain et al. 2010), and AMCOR well 6011 (Hathaway et
210 al. 1979) were used to categorize the sediments into three facies types based on density logs.
211 Mountain et al. (2010) reported that density measurements corresponded to lithological changes
212 observed on core data. Therefore, we defined the following categories: sand ($\rho > 2\,050\text{ kg m}^{-3}$),
213 silt ($1\,820\text{ kg m}^{-3} \leq \rho \leq 2\,050\text{ kg m}^{-3}$) and shale ($\rho < 1\,820\text{ kg m}^{-3}$). The categorized well
214 logs are shown in Figure 3. It must be noted that well 6011 is a projected well, which is
215 approximately 10 km offset from the model transect. Despite this lateral offset, we assume the
216 lithological information derived from the well can be considered representative for the sediment
217 column in the proximal part of the shelf. Including this well data in the stochastic modelling
218 process introduces an additional control point and reduces the uncertainty in the proximal part of
219 the shelf.

220

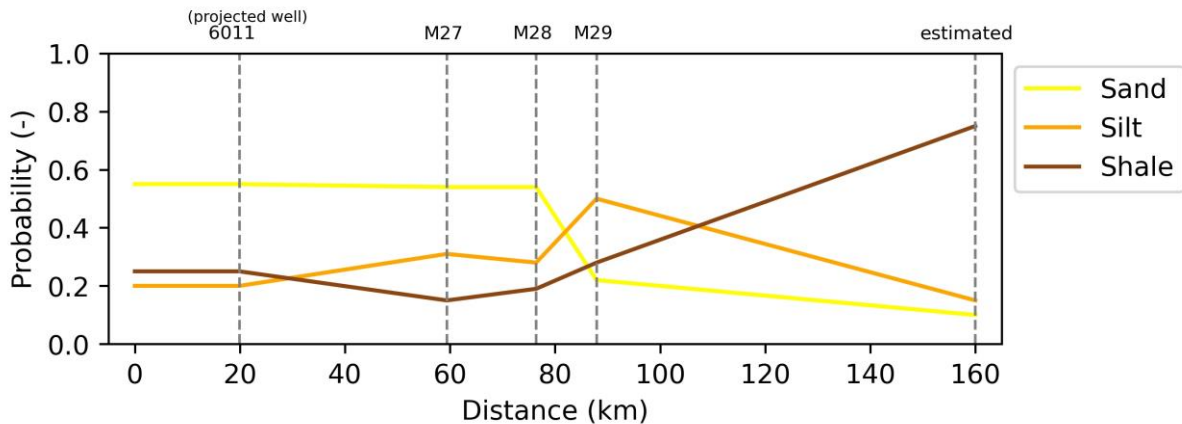


221

222 *Figure 3 Interpretation and categorization of lithologies from bulk density data at well sites 6011, M27, M28, and M29. Mountain*
 223 *et al. (2010) reported that density variations in IODP Expedition 313 wells broadly correspond to lithology.*

224 The categorized well log data were used to derive 1D facies probability functions. The horizontal
 225 facies probability function was defined by linear interpolation of control points, each
 226 corresponding to a single well. We calculated the probability of occurrence of each category over
 227 the entire well. This probability was defined for each facies category as $P_i = n_i/n_T$, where n is the
 228 number of samples of the category denoted with subscript i , and n_T is the total number of samples.
 229 In the absence of well data, a distal control point was assigned at the boundary of the model
 230 domain. At this location, we assume $P_{\text{shale}} = 0.75$, $P_{\text{sand}} = 0.1$ and $P_{\text{silt}} = 0.15$. This method of using

231 the proportion of each facies is a standard approach to incorporate geological trends into stochastic
 232 models (Deutsch and Pyrcz 2014). In deltaic environments like the New Jersey shelf, it is typical
 233 that fine-grained sediments are transported further basinward, resulting in a general offshore fining
 234 trend in the lithology (i.e., increasing probability of shale). The trends obtained from four wells is
 235 shown in Figure 4.



236

237

Figure 4 Horizontal facies probability functions calculated by linear interpolation between control points.

238 The horizontal trends were assigned globally for the model domain. Vertical trends were
 239 incorporated by calculating vertical proportionality curves for each sequence individually using
 240 well data analysis tools in Petrel. These trends jointly constrain the sequential indicator simulation
 241 algorithm and incorporate realistic geological features into the suite of models produced. The
 242 model domain is thereby populated with the three facies types, to which petrophysical properties
 243 were later assigned for numerical simulation. Cemented intervals identified by core analysis
 244 presented in Lofi et al. (2013) were included deterministically in the model framework. These
 245 high-density intervals lead to high acoustic impedance at the cemented regions of the sequence
 246 boundaries (Miller et al. 2013a). We approximate the lateral extent of these cemented layers based
 247 on the interpretation presented in Lofi et al. (2013) as well as the amplitude of the reflectors.

248 The final input to the stochastic model are the variogram parameters. In the absence of sufficient
 249 well data for variogram modelling, we estimate the variogram parameters based on the
 250 depositional model. The New Jersey clinothem system is penetrated at the topset, rollover and
 251 bottomset positions by IODP wells M27, M28 and M29 respectively (Mountain 2010). This system
 252 of prograding clinoforms is at least 22 km across and interpretation of sequences across the wells

253 has been established based on seismic data (Miller et al. 2013b), as well as biostratigraphic
 254 interpretation (Browning et al. 2013). Generally speaking, the dimensions of shoreface-shelf
 255 deposits for wave-dominated delta system have a wide range from a few kilometres up to 30 km
 256 (Hampson 2010; Reynolds 1999). The continuity of facies along the dip direction is determined
 257 by the shoreline progradation distance of the delta during the time of deposition. Using this model,
 258 we assigned a correlation length of 15 km for the variogram model as an average representative
 259 value for the entire system. In addition to the correlation length, we defined a dip angle of
 260 maximum correlation for each sequence. This was determined from the average dip of the seismic
 261 reflectors in the sequence. These values ranged between 0.25° and 1.2° .

262 The matrix properties were assigned to the model domain based on the interpreted lithology.
 263 Porosity compaction trends were derived from core-sampled porosity data measured by Mountain
 264 et al. (2010). The data of each facies group was fitted to an empirical exponential equation first
 265 described by Athy (1930):

$$266 \quad \theta = \theta_0 e^{-az} \quad (1)$$

267 where θ is the porosity at depth z (m), θ_0 is the initial porosity and a is the correlation coefficient.
 268 Two trends were derived based from the log data, a sand compaction trend and a silt/shale
 269 compaction trend. The three categories sand, silt and shale correspond to high, medium and low
 270 permeability, respectively. Matrix parameters are summarized in Table 1.

271

272

273

Table 1 Summary of matrix properties used in all simulations

Parameter	Value	Unit	Reference
Permeability	† 9.4×10^{-12} * 7.4×10^{-14} †† 9.0×10^{-16}	m^2	(Lofi et al. 2013; Thomas et al. 2019)
Porosity	† $44.7 e^{-2.46 \times 10^{-4} z}$ $57.5 e^{-5.93 \times 10^{-4} z}$	-	(Mountain et al. 2010; Thomas et al. 2019)
Thermal conductivity	†2.9 *2.3 ††1.7	$\text{W m}^{-1} \text{K}^{-1}$	(Mountain et al. 2010)
Volumetric Heat capacity	† 2.4×10^6 1.9×10^6	$\text{J K}^{-1} \text{m}^{-3}$	

274

† - sand, * - silt, †† - shale

275

276 **2.2 Stochastic simulation and model selection**

277 The SIS algorithm generates multiple stochastic realizations of equally probable scenarios, which
278 honour the input data. However, SIS does not consider the connectivity of the model domain. The
279 lateral flow connectivity is an important consideration in assessing the hydrogeologic evolution of
280 the freshened groundwater reservoirs on the New Jersey shelf, and the potential role of modern
281 day recharge. Connectivity of stochastic models are often assessed by calibration of facies
282 distribution with field pumping data (Zhou et al. 2014). In the absence of such data for our study
283 domain, we conducted a simple Monte Carlo sampling from a suite of 100 model realizations to
284 select models to use for numerical simulations (Deutsch and Pyrcz 2014).

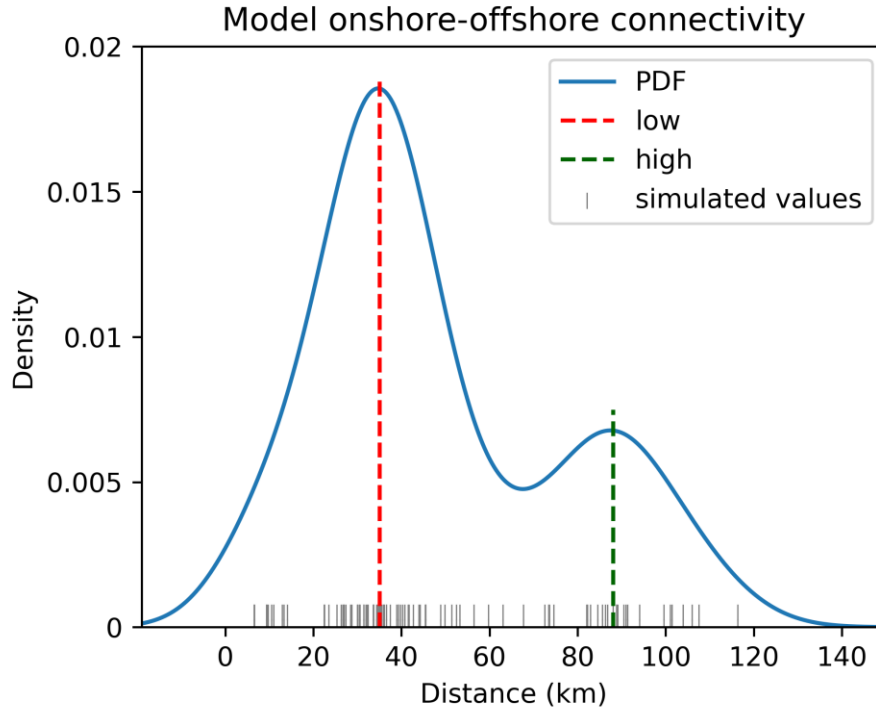
285 The steady-state solution of the hydraulic head was used to derive a simple metric that is related
286 to an important aspect of the system, the onshore – offshore connectivity of the realization. This
287 process-based model selection approach is a standard practice in geostatistical reservoir modelling
288 (Deutsch and Pyrcz 2014). The models were initiated with hydrostatic conditions, and fixed head
289 boundary conditions at the lateral boundaries such that a 25 m hydraulic head difference was
290 maintained between the landward and oceanward boundaries. That value was chosen based on
291 results presented in Cohen et al. (2010), which estimated that conditions during the LGM resulted
292 in head values along the New Jersey that may have been 25 m higher than present-day. After
293 calculating the steady-state solution, the horizontal distance between the land boundary and the
294 average position of the contour representing a 10 m increase in head within the model domain was
295 measured. A longer distance would correspond lower hydraulic gradient, an indication of higher
296 flow connectivity between two points (Freeze and Cherry 1979). Based on the probability
297 distribution of this distance, two model realizations were chosen for numerical simulations
298 representing high- and low onshore-offshore connectivity scenarios. Numerical simulations were
299 performed on both model scenarios.

300

301 Summary statistics calculated on the lateral distance to the 10 m contour line show an average
302 distance of 48.4 km with a standard deviation of 27 km. The probability density function (PDF)
303 was estimated using a gaussian kernel density estimation (Hastie et al. 2009). This is a non-
304 parametric method that estimates the PDF of a continuous random variable. The PDF shown in

305 Figure 5, has a bimodal distribution, which points to low-to-intermediate connectivity as the more
 306 likely scenario given the currently available data. A less likely scenario is high connectivity.

307

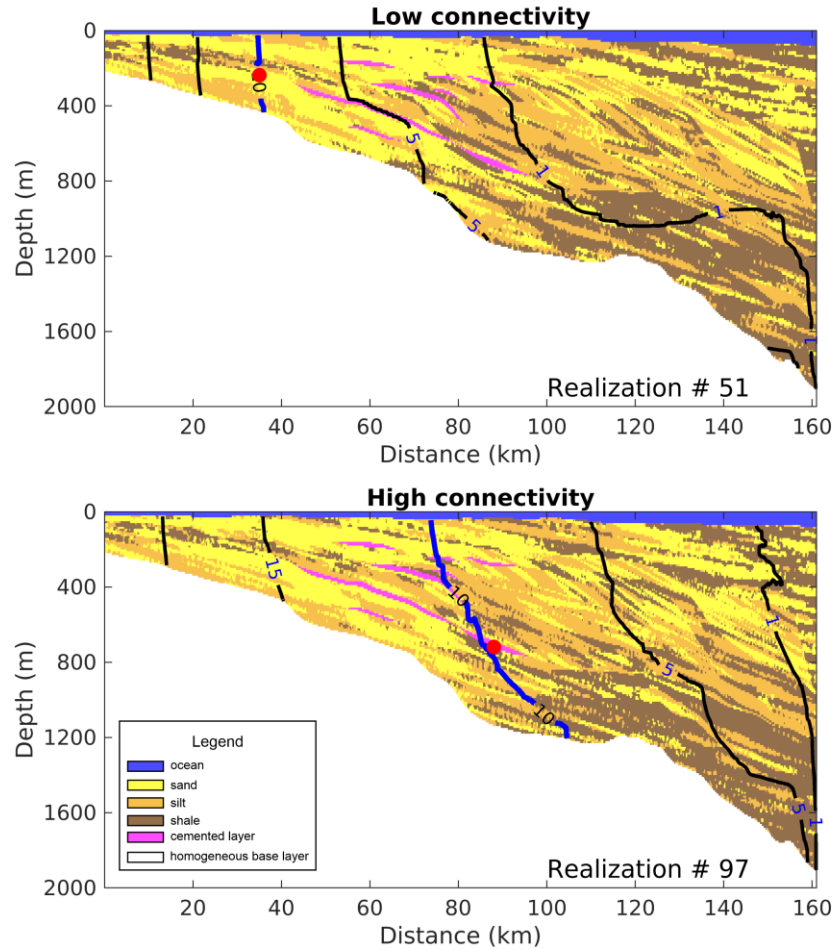


308

309 *Figure 5 Probability density function of model connectivity metric showing a bimodal distribution for a suite of 100 stochastic*
 310 *model realizations. The positions of the low and high onshore-offshore connectivity modes are indicated by red and green dashed*
 311 *lines, respectively. The realizations with values closest to these two modes were selected for numerical simulation.*

312 Based on these summary statistics, we conducted numerical studies using two realizations,
 313 representing low and high connected mode scenarios. The models with the connectivity values
 314 closest to the two modes were selected. The high and low connectivity scenarios were represented
 315 by realizations 97 and 51, respectively. These realizations are shown side by side in Figure 6. The
 316 steady-state hydraulic head contours are overlaid on the model domain.

317



318

319 *Figure 6 (a) Low onshore-offshore connectivity model (b) High onshore-offshore connectivity model realizations. Both models*
 320 *show the position of the 10 m hydraulic head contour in bold blue. The models were ranked based on the horizontal distance*
 321 *between the landward boundary and the average position of the contour indicated by the red dot. The corresponding porosity*
 322 *compaction models are included in the Supporting Information of this manuscript (Fig. S1)*

323

324 **2.3 Modelling the offshore freshened groundwater system**

325 Numerical simulations were performed using a finite difference numerical modelling algorithm
 326 called SHEMAT-Suite (Clauser 2003; Keller et al. 2020; Rath et al. 2006). We simulate variable-
 327 density groundwater flow coupled with heat transport, taking into consideration the key drivers of
 328 fresh/saline groundwater flow on this regional scale model. Clauser (2003) provides a detailed
 329 description of the partial differential equations implemented in SHEMAT-Suite for groundwater
 330 flow, heat and solute transport. The parameters assigned to the flow model are the same as in
 331 Thomas et al. (2019). These are summarized in Table 2.

332

333

Table 2 Summary of model parameters used in all simulations

Parameter	Value	Unit	Reference
Fluid properties	Reference Density (freshwater)	1 000	kg m ⁻³
	Compressibility	4.58×10^{-10}	Pa ⁻¹
	Viscosity	1.0×10^{-3}	Pa s
	Thermal Conductivity	0.6	W m ⁻¹ K ⁻¹
	Specific heat capacity	4128	J K ⁻¹ kg ⁻¹
Solute transport	Molecular Diffusion Coefficient	1.1×10^{-9}	m ² s ⁻¹
	Molar Mass (NaCl)	58.44	g mol ⁻¹
	Dispersivity	50	m

334

335 We simulated 70 000 years of the Pleistocene lowstand. During this period, the sealevel fell as low
 336 as 120 m relative to present-day (Imbrie et al. 1984). As a result, large areas of land were
 337 subaerially exposed on the low-angle passive margin platform of the New Jersey shelf. For the
 338 purpose of this analysis, we define two distinct phases of this period. The recharge phase from 70
 339 000 to 12 000 years BP, and the flooding phase from 12 000 years BP to present day. That starting
 340 point was chosen as it is approximately when the entire transect of the ocean floor (Figure 2)
 341 became subaerially exposed. A set of idealized simulations were designed to investigate the
 342 sensitivity of freshwater emplacement as hydraulic conditions on the shelf responded to sea-level
 343 lowstand.

344 The numerical study is presented in two phases. Firstly, we assess the model sensitivity to
 345 topographic-driven flow (base case), cemented intervals, enhanced terrestrial discharge and
 346 permeability anisotropy. Topographic-driven flow refers to the lateral hydraulic gradient induced
 347 by the seafloor topography. We consider this the base case, as the shelf exposure is the essential
 348 condition that allows meteoric recharge. The cemented intervals have been identified in core
 349 samples, and found to be correlated with the fresh – saline pore fluid boundaries reported in
 350 previous petrophysical studies (Lofi et al. 2013; Mountain et al. 2010). We simulated a
 351 hypothetical scenario in which these intervals were assigned regular matrix properties of silt (Table
 352 1), in order to quantify their impact. Enhanced terrestrial discharge (ETD) refers to offshore-
 353 directed flow generated at the landward boundary of the model, accounting for a subterranean
 354 influx of freshwater. This was modelled by an increased hydraulic head at that boundary. The

355 assigned value was based on computed heads during the Pleistocene and Holocene along the
356 Atlantic continental shelf modelled by Cohen et al. (2010). Their simulations accounted for
357 conditions induced by ice sheet loading and sealevel fall, and estimated up to 25 m increase in
358 hydraulic head on-shore in the region near our model transect. Finally, we investigate the influence
359 of anisotropic permeability. Anisotropy is a common feature in sedimentary environments due to
360 the influence of bedding and possible compaction banding (Holcomb and Olsson 2003; Vajdova
361 et al. 2004). In this study, we define the anisotropy in terms of the ratio of horizontal permeability,
362 k_h and vertical permeability, k_z . We consider two plausible values of the anisotropic ratio, two and
363 ten. The set of simulations described above was conducted on both high and low connectivity
364 model realizations. Boundary conditions for all scenarios are summarized in the following section.
365 The scenarios were compared based on three observation criteria. Firstly, the volumetric trend of
366 fresh pore fluid in the model domain over the simulated time. Although the model is 2D, the
367 volumes were calculated based on the cell with of 100 m, and the pore volume of each cell.
368 Secondly, the present-day pore fluid concentration profiles were compared to measured data at the
369 four wells sites for each scenario. Finally, the pore fluid concentration distribution in the model
370 domain was analysed at two key times, the end of the recharge phase and at present day to consider
371 the role of geological heterogeneity.

372 In the second phase, we conduct a comprehensive set of simulations on a single representative
373 model realization, designed to reconstruct conditions over the period from 70 000 years BP to
374 present-day. For this phase, we consider only the low onshore-offshore connectivity realization
375 (Fig 6 a), as it corresponds to the highest likelihood based on the probability distribution (Fig. 5).
376 We consider the compounded effect of topographic-driven flow, enhanced terrestrial discharge
377 and permeability anisotropy. At the end of these simulations, the pore fluid concentration in the
378 model domain was compared to present-day observations in IODP Expedition 313 wells and
379 AMCOR well site 6011. This comparison, together with the distribution of freshened groundwater
380 in the model domain is analysed to draw conclusions about the dynamic nature of the OFG system.

381 The volume of freshwater in the model domain over time is considered as a metric for quantifying
382 the influence of the abovementioned factors. Ocean water has a total dissolved solid (TDS)
383 concentration of approximately 35 g L^{-1} . For the purpose of this study, the modelled solute is NaCl,
384 which has a molar mass $58.443 \text{ g mol}^{-1}$. This translates to, and is specified in SHEMAT-Suite as

385 a molecular concentration of 0.6 mol L^{-1} . In this study, pore fluid is defined as freshwater when it
386 has a solute concentration of less than 0.3 mol L^{-1} , i.e., approximately half the TDS concentration
387 of seawater ($\sim 17.5 \text{ g/L TDS}$).

388 **2.3.1 Initial and boundary conditions**

389 The coupled variable-density flow and heat transport simulations in this study require compatible
390 boundary conditions for groundwater flow, heat and solute transport. The boundary conditions
391 were designed to be consistent with laws of conservation of mass and energy within the model
392 domain. All simulations were initialized under the same conditions to facilitate comparison.

393 The initial temperature and hydraulic head distribution in the model domain were set to the steady-
394 state solution of their respective equations. For temperature, surface cells were assigned a Dirichlet
395 boundary condition of $4 \text{ }^\circ\text{C}$, representing the average surface temperature during the recharge
396 phase (Johnsen et al. 1995). Basal specific heat flow was prescribed by a Neumann boundary
397 condition of 0.06 W m^{-2} (Lachenbruch and Sass 1977). The groundwater flow was constrained by
398 a Dirichlet boundary condition assigned along the surface cells and lateral boundaries. The head
399 in each surface cell was set to its elevation relative to the model datum. At the landward and
400 oceanward boundaries, the head was set to the elevation of their respective surficial cells. We
401 invoke the simplifying assumption that the hydraulic gradient mirrors the surface topography, and
402 consider only saturated flow (Freeze and Cherry 1979). Determining initial salinity distribution is
403 challenging as the position of the freshwater – seawater interface is transient and dynamic (Meisler
404 et al. 1984). We assume the domain is fully saturated with saline pore fluid (0.6 mol L^{-1} or 35 g L^{-1}
405 TDS) in all cells below sealevel, shown in Figure 7. This represents a conservative initial estimate
406 as it is likely that more freshwater recharge would have taken place as the transect was partially
407 exposed i.e., prior to our simulated period. Therefore, the model may underestimate the volume of
408 freshwater that would have been emplaced over the entire regressive – transgressive cycle. This
409 initial condition has also been implemented in a comparable regional numerical study (Siegel et
410 al. 2014). The assumption isolates the simulated period as a minimum baseline for recharge, and
411 provides a reference point from which to ascertain whether older freshwater emplacement is
412 needed to explain the present-day observations.

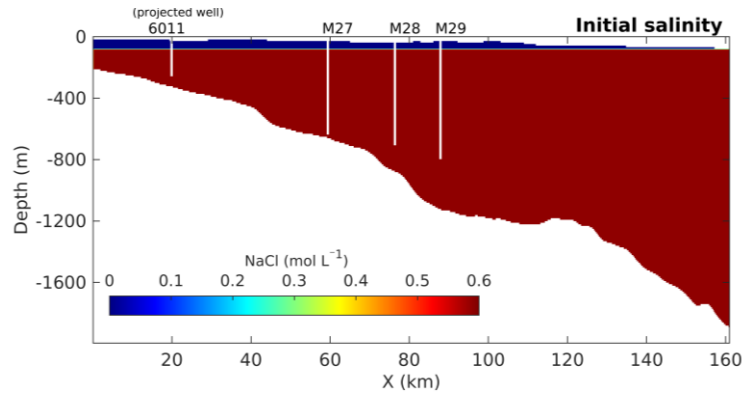


Figure 7 Initial salinity distribution in model domain. All cells below initial sealevel initialized at $0.6 \text{ mol L}^{-1} / 35 \text{ g L}^{-1}$ TDS

413

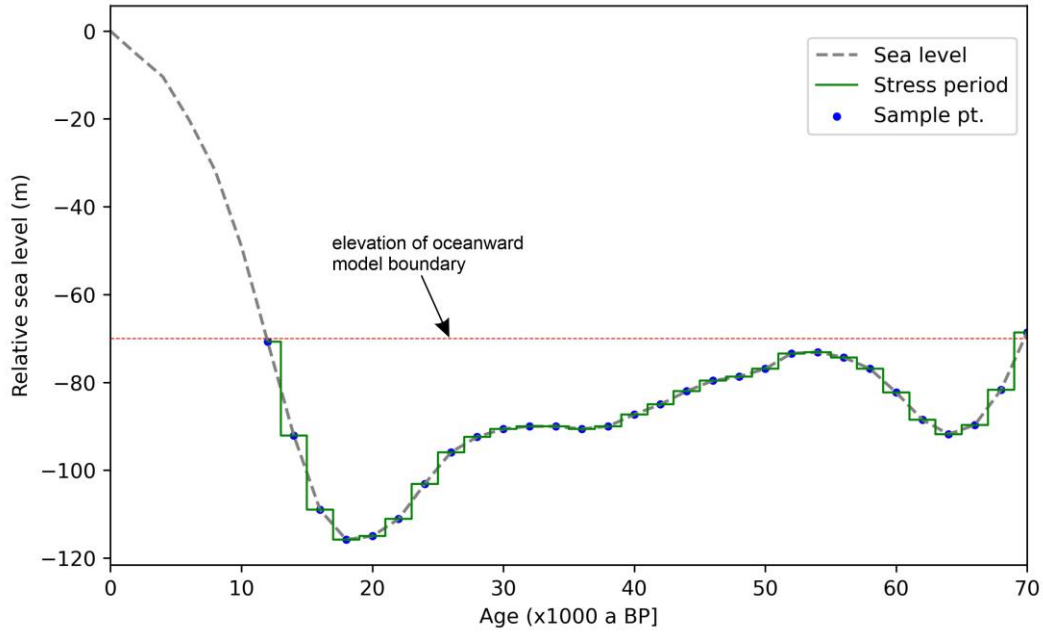
414

415 During the recharge phase, surface temperature was fixed to the initial condition described above,
 416 with the steady-state thermal gradient at the lateral boundaries. Dirichlet boundary condition of
 417 zero salinity was assigned to the model surface. This represents meteoric recharge, which is known
 418 to have negligible salinity (Selley and Sonnenberg 2015). The landward and oceanward lateral
 419 boundaries were set to 0.0 mol L^{-1} and 0.6 mol L^{-1} , respectively. The hydraulic head at the surface
 420 and landward boundaries were set to the surface elevation. The unsaturated zone and associated
 421 infiltration processes are assumed to be negligible. This assumption is validated considering the
 422 large aspect ratio between the model length and the depth of the sediments under investigation
 423 (Freeze and Cherry 1979).

424 At the oceanward boundary, we assigned a time-varying Robin boundary condition. This specifies
 425 flow across the model boundary using the formulation as described in Jazayeri and Werner (2019):

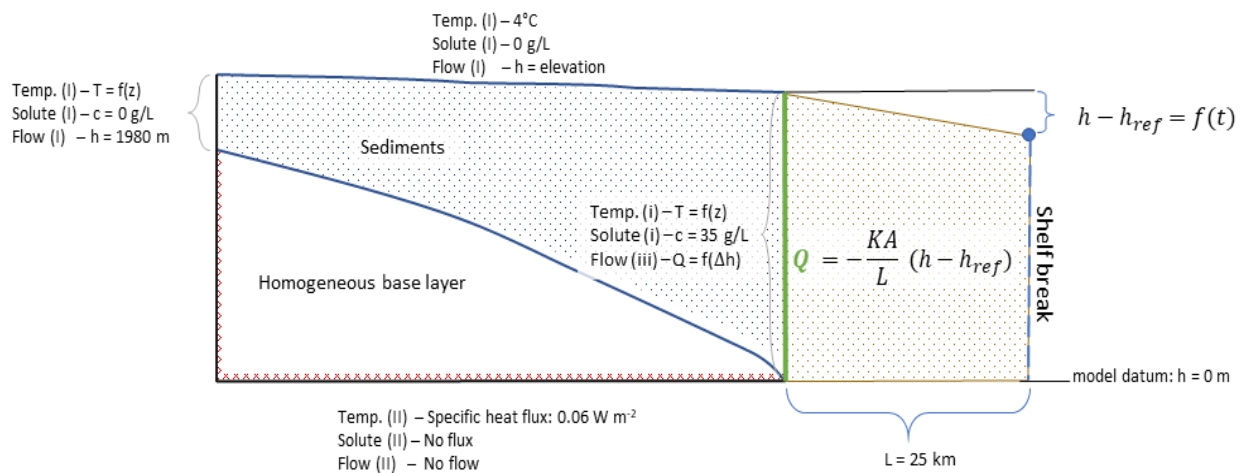
$$426 \quad Q = -\frac{KA}{L} (h - h_{\text{ref}}) \quad (2)$$

427 where $K \text{ (m s}^{-1}\text{)}$ is the hydraulic conductivity of the extended region, A is the cross-sectional area
 428 of the boundary, $h - h_{\text{ref}} \text{ (m)}$ is the head drop between the model boundary and an external
 429 reference point and $L \text{ (m)}$ is the distance between the model boundary and that point. The reference
 430 head, h_{ref} is the sealevel elevation at the shelf edge. The values were sampled from the relative
 431 sealevel curve by Imbrie et al. (1984) at 2000 year intervals, as summarized in Figure 8. This type
 432 of boundary condition is applied as our model transect does not extend all the way to the shelf
 433 edge. This head dependent flux approximates the hydraulic conditions of the shelf region outside
 434 of the model domain.



435
 436 *Figure 8 Relative sea level curve of the past 70 000 years used to determine boundary conditions for model domain. Blue dots show*
 437 *the sample points (h_{ref}) and light green lines indicate 2000 year period for which the value was applied. The red dashed line*
 438 *represents the level of the model's oceanward boundary (h).*

439 For our model domain, $A = 1.92 \times 10^5 \text{ m}^2$ based on the cell dimensions, and the distance from
 440 the model boundary to the shelf edge $L = 25\ 000 \text{ m}$. We estimated a value of $K = 7.6 \times 10^{-8} \text{ m}$
 441 s^{-1} as the average hydraulic conductivity for the distal section of the shelf. The main model
 442 boundary conditions during the recharge phase are summarized in Figure 9. The conditions were
 443 applied in all cases with the exception of ETD. In that scenario, shore-parallel flow was enhanced
 444 by increasing the head at the landward boundary by 25 m.
 445



446
 447 *Figure 9 Recharge boundary condntions. (i) Dirichlet type boundary conditions, (ii) indicates Neumann type boundary conditions, and*
 448 *(iii) Robin boundary condition. Red hashed line represents no flow conditions assigned to the homogeneous base layer.*

449 Flooding Phase

450 During the 12 000-year period of Holocen transgression, the topographic flow regime of the
451 recharge phase passes over into today's hydrostatic conditions. Each model run was initialized
452 using pore fluid concentration obtained at the end of the corresponding recharge phase. Time-
453 dependent boundary condition functions were implemented in SHEMAT-Suite to represent a
454 transgressing coastline during the simulated period. The hydraulic head at surface cells was
455 increased to sea-level elevation as the model domain is gradually flooded. The head at the
456 oceanward boundary was initiated at the surface elevation and increased over the transgressive
457 period to the present-day sea level at that point of the shelf. The head at the landward boundary
458 was set to 5 m above surface elevation. The salinity of the relevant surface nodes was increased to
459 ocean salinity according to the timing of the marine transgression. The surface temperature was
460 also increased linearly from 4 °C to the present-day average sea-surface temperature of 14 °C
461 (O.S.P.O. 2013). Temperature at the lateral boundaries was fixed to the steady-state thermal
462 gradient.

463

464 **3 Results**

465 **3.1 Numerical simulation of freshwater emplacement**

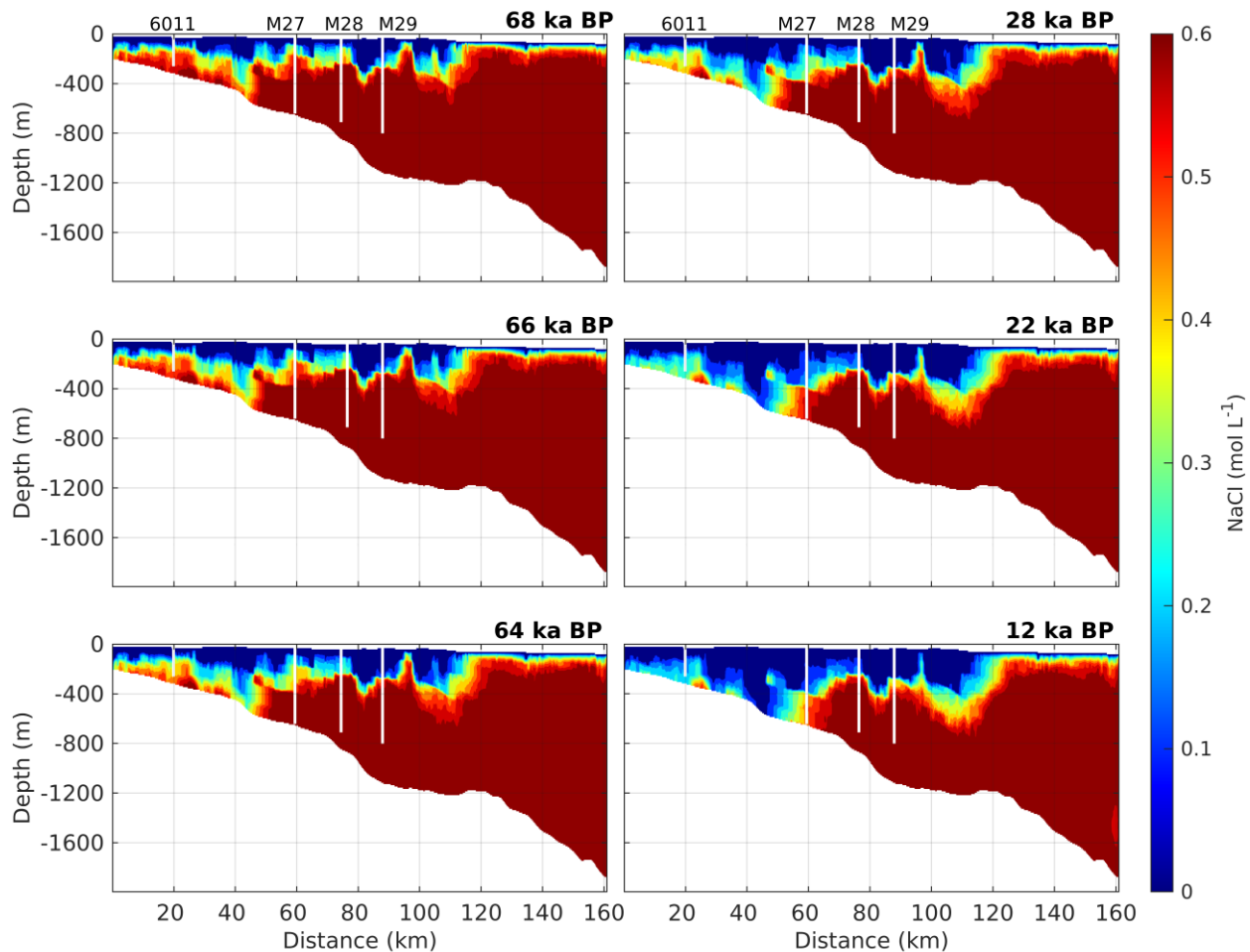
466 In the following sections the results of the numerical simulation are presented in detail. Firstly, we
467 present observations of the freshwater emplacement mechanism in the context of a heterogeneous
468 shelf model. This is followed by sensitivity analysis comparing the influence of various
469 hydrogeologic scenarios. Finally, we present a paleo-hydrogeological reconstruction of the LGM
470 on a representative shelf model.

471 **3.1.1 Analysing the mechanism of freshwater emplacement**

472 This section presents the results of topographically driven flow for both high and low onshore-
473 offshore connectivity cases, abbreviated as HC and LC, respectively. The mechanisms by which
474 freshwater is emplaced in the sediments are analysed in the context of the heterogeneous shelf
475 models.

476 Figure 10 shows the progressive freshening of the shelf sediments in the base case in the low
477 onshore-offshore connectivity model. The figure shows snapshots of the recharge phase taken in
478 the periods between 68 ka BP to 64 ka BP, and 28 ka BP to 12 ka BP. These correspond to the
479 periods of most rapid sealevel change (see Fig. 8) and the most observable changes in pore fluid
480 concentration. It can be observed that due to topographically driven flow during the simulated sea-
481 level lowstand, freshwater is emplaced across the entire shelf transect to varying depths. The
482 interface between fresh and saline water is highly complex as a result of the geological
483 heterogeneity. The depth of freshening becomes gradually more shallow in the oceanward
484 direction. The result indicates that the offshore directed hydraulic gradient resulting from surface
485 topography is sufficient to drive freshwater into sediments across the entire shelf transect. The
486 most distal part beyond 120 km from the shore is relatively flat, leading to much slower rates of
487 freshening. In general, a downward movement of the fresh – saline interface occurs in response to
488 a sea-level lowstand. Top-down freshening by surface derived recharge appears to be the primary
489 mechanism driving the emplacement of freshwater. In a topographically driven flow regime, the
490 recharge is focussed into high permeability intervals (Hobbs and Ord 2015). As a result of the
491 hydraulic gradients, recharged freshwater is driven laterally into aquifer units, while overlying

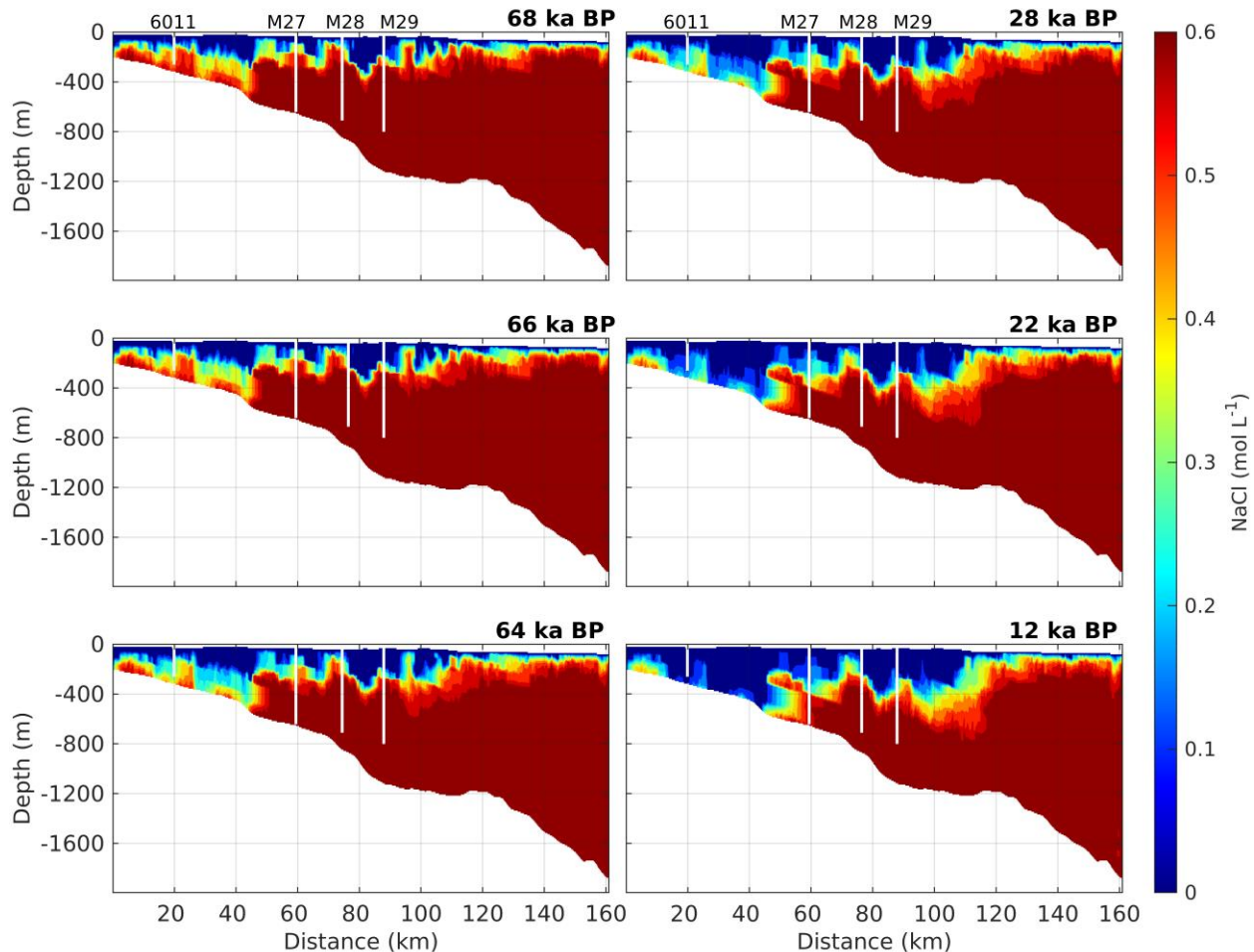
492 confining units remain saline for a longer period. Furthermore, this preferential flushing of
 493 permeable intervals causes density instabilities, resulting in density-driven free convection
 494 between the saline pore fluid in the confining units and the underlying freshened aquifer units.



495

496 *Figure 10 Solute concentration in the model domain during the recharge phase for the base case scenario in the low onshore-*
 497 *offshore connectivity model realization. Snapshots of the transient results show the complexity of freshwater recharge in the*
 498 *heterogeneous subsurface. Freshening occurs by a combination of advective flow in aquifer units and density-driven free convection*
 499 *in confining units. Freshening appears to occur primarily from the surface recharge.*

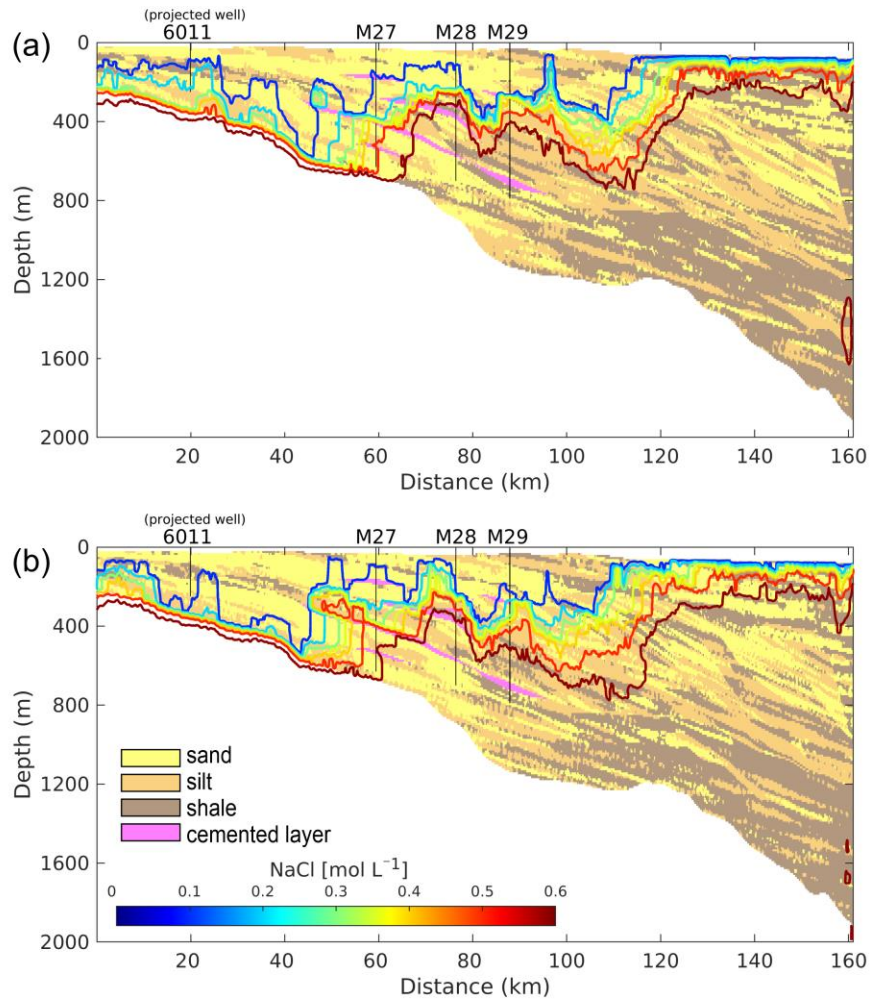
500 The recharge phase displays similar dynamics in the high onshore-offshore connectivity model,
 501 shown in Figure 11. These results indicate that the recharge of freshwater during lowstand is
 502 primarily a function of topography and geological heterogeneity. Marginal changes in the pattern
 503 of freshening can be seen in the proximal part of the shelf as a result of the higher onshore-offshore
 504 connectivity. However, the general position and shape of the fresh – saline water interface closely
 505 match the LC model.



506
 507 *Figure 11 Solute concentration in the model domain during the recharge phase for the base case scenario in the high onshore-*
 508 *offshore connectivity model realization. The distribution at the end of the recharge phase (12 ka BP) shows more evidence of*
 509 *channelized flow of freshwater when compared to the low connectivity case. Top-down freshening by surface recharge is*
 510 *restricted by laterally continuous aquitards present in this model.*

511 The pore fluid concentration at the end of the recharge phase is shown for both models in Figure
 512 12. It can be observed that freshwater is driven deeper in proximal regions of the shelf, where the
 513 sediment column is primarily sandy. Toward the distal shelf regions, there is a decreasing trend in
 514 grain size, which correlates with shallower penetration of freshwater. The shape of the fresh –
 515 saline interface shows considerable lateral variability corresponding to the stratigraphic
 516 terminations of sandy units. This highlights the importance of capturing the sequence stratigraphic
 517 architecture. A local topographic high around 100 km also corresponds to relatively deeper
 518 penetration of freshwater recharge. As surface elevation increases inland, freshwater is driven
 519 deeper into the sediment column. Freshwater was driven as deep as 500 m in the region of IODP
 520 well M27, both high- and low-permeability intervals are completely flushed with freshwater. The
 521 region around M28 shows freshwater recharge occurring down to about 300 m depth. Deeper

522 freshening appears to be impeded by the presence of cemented and low-permeability intervals
 523 below 300 m.
 524



525
 526 *Figure 12 (a) Low onshore-offshore connectivity, (b) High onshore-offshore connectivity. Pore fluid concentration contours in model*
 527 *domain at the end of the recharge period (i.e. 12 000 years BP) overlaid on the facies model highlighting the correlation between*
 528 *geological heterogeneity and the distribution of freshwater recharge.*

529 The presence of low-permeability sediments near the surface is a feature of the subsurface
 530 heterogeneity that strongly influences freshwater recharge. The HC model, shown in Figure 12 b,
 531 features some near-surface shale intervals in the mid-shelf region between 50 km – 80 km which
 532 are absent in the LC model. While these aquitards create conduits that increase the lateral flow
 533 connectivity in the model domain, they also have the effect of reducing the depth of penetration of
 534 surface derived recharge. This influences the extent to which the underlying sediments are
 535 freshened in the HC model relative to the LC model. The effect can also be observed in the
 536 proximal region of the models where more freshening occurs in the HC model due to

537 discontinuities in the confining layers. The near-surface distribution of low-permeability
538 sediments influences the emplaced freshwater volumes such that the LC model facilitates more
539 recharge relative to the HC model. The relative volumetric trends are presented in the following
540 section.

541 **3.1.2 Sensitivity analysis**

542 Freshwater volumetric trends

543
544 In this section we present the simulation results for all scenarios in the high onshore-offshore
545 connectivity (HC), and the low onshore-offshore connectivity (LC) models. We compared the two
546 model realizations based on three sets of observation: (1) freshwater volume trends over the
547 simulated period, (2) fluid concentration at the end of the recharge phase and present-day, and (3)
548 fit between observed and measured pore fluid concentration at well locations.
549

550
551 Figure 13 shows the freshwater volume trend for the 70 000 year simulated period in both model
552 realizations. There are two periods of rapid increase in freshwater emplacement that coincide with
553 rapid sea-level fall. These occur from 70 000 years BP to 60 000 years BP and about 28 000 years
554 BP to 18 000 years BP. The time of relatively slower regression between these two periods is
555 characterized by a gradual linear increase in the freshwater volume. This pattern is replicated in
556 both the HC and LC model realizations. A key observation is that all the curves show a similar
557 trend to the base case. This suggests that the dominant mechanisms during the lowstand are
558 meteoric recharge and topographically driven flow.

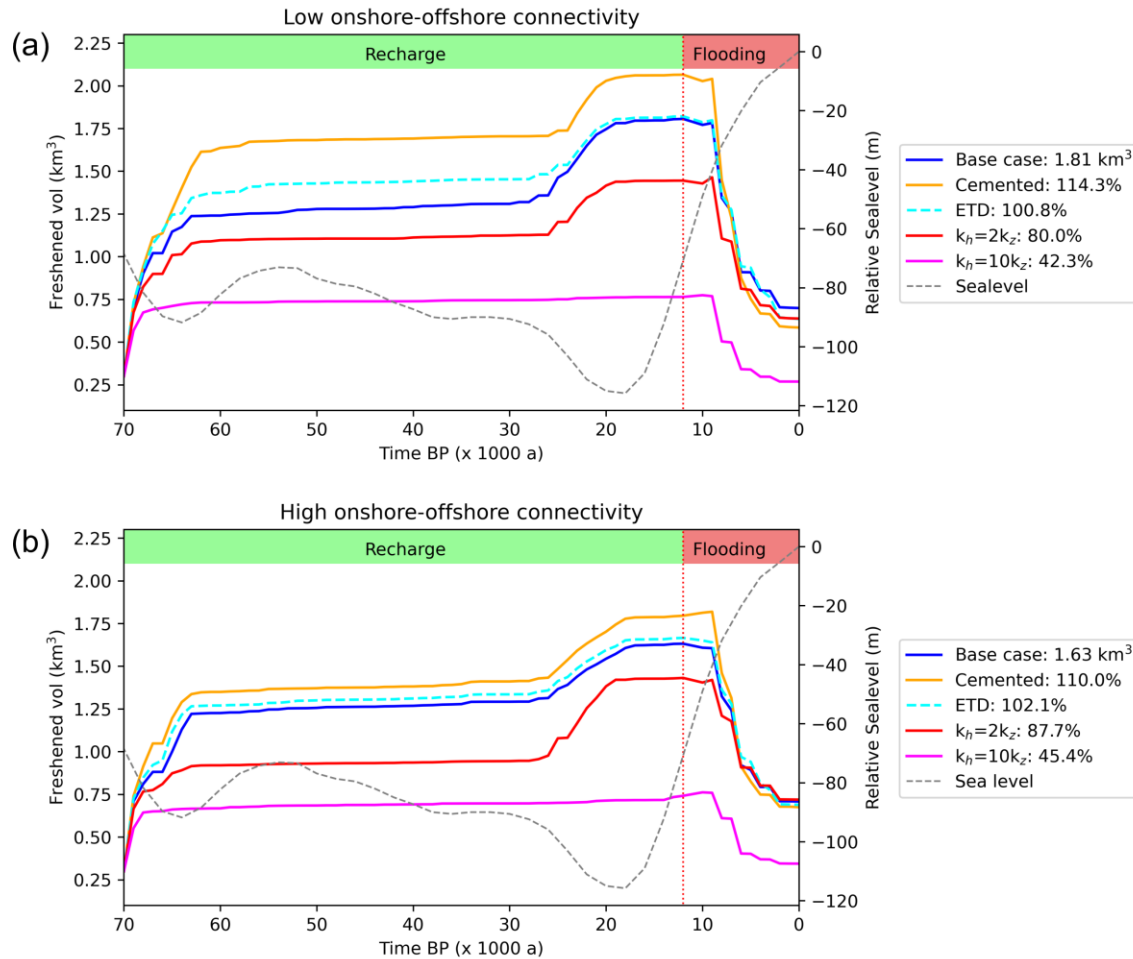
559
560 Removing the cemented intervals resulted in a moderate increase in emplaced freshwater relative
561 to the base case (10 % - 14 %). The volume that survived until present day was only marginally
562 smaller than the base case (blue curves in Fig. 13). This suggests that while cemented intervals
563 strongly influence the geometry of surviving freshwater reservoirs, they are not significantly more
564 influential than low-permeability shales on the overall reservoir volumes.

565
566 The ETD scenario resulted in a 2.1 % increase in the freshwater volume for the HC model and <
567 1 % in the LC model realization. This result is consistent with the difference in onshore-offshore
568 connectivity between both models. In our model domain, the sediment column on the landward

569 boundary is 300 m thick, therefore this may underestimate the amount of discharge that enters into
570 the offshore environment e.g., through deeper connected pathways.

571

572 The anisotropic permeability scenarios had the most significant influence on the emplaced
573 freshwater volume. In the case of a horizontal to vertical ratio of two, the freshwater volume was
574 reduced by 20 % in the LC model and 12.3 % in the HC model, relative to the base case. In both
575 models the present-day freshwater volume is approximately equal to the base case. The anisotropy
576 reduces the emplaced volume, but also acts to preserve more of the emplaced freshwater during
577 subsequent regression. An increase of the anisotropy ratio to ten, led to a further decrease in the
578 emplaced volumes and a significant flattening of the volumetric trend. We observed a very
579 dampened response to the periods of rapid sea-level fall. In that case, the freshwater volume was
580 reduced by 57.7 % in the LC model and 54.6 % in the HC model relative to the respective base
581 cases. In the presence of strong anisotropy, effectively all of the recharged freshwater is salinified
582 during the subsequent flooding phase, as shown by the magenta colored curves in Figure 13. These
583 observations highlight the significance of downward infiltration of meteoric recharge through the
584 sediment column from the model surface.



585 Figure 13 The volume of freshwater over the simulated period is plotted for all scenarios in (a) LC model and (b) HC model. The
 586 legend shows the volume of freshwater emplaced during the recharge phase for the base case, and the relative percentages at the
 587 end of the recharge phase are shown for all other scenarios. The dashed grey line shows the sea-level curve after Imbrie et al.
 588 (1984) plotted on the secondary y-axis (right).
 589

590 Model concentration distribution

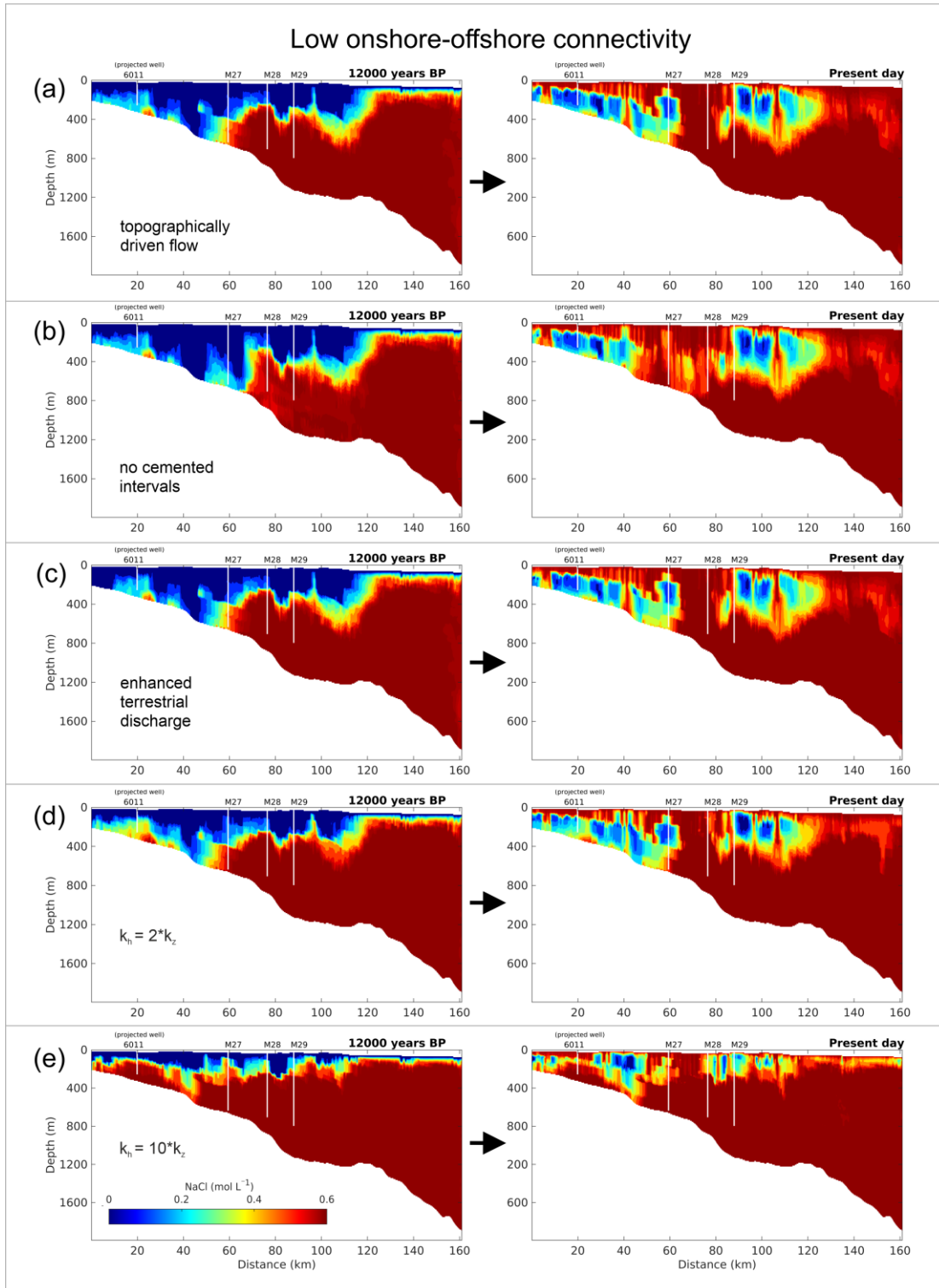
591

592 The distribution of pore fluid concentration in the model domain is shown at two key times i.e.,
 593 the end of the recharge phase at 12 000 years BP, and present-day. We present results of the low
 594 onshore-offshore connectivity model in Figure 14, where each panel displays a different simulated
 595 scenario. In the recharge phase, we can observe that more freshening occurs in the region of M27
 596 in the absence of cemented intervals (Figure 14 b). The ETD scenario shows only minor changes in
 597 the distribution within a range of 20 km from the landward boundary (Figure 14 c). Figure 14 (d) and
 598 (e) show the low and high anisotropy ratio cases, respectively. These result in an upward shift and
 599 general flattening of the fresh-to-saline interface. In the case of high anisotropy, freshening only
 600 occurs to ~ 300 m. With the exception of the high permeability scenario, the present day

601 distributions consistently reproduce a seaward-dipping zone of fresh water extending from the
602 landward boundary to ~ 40 km offshore. Downward fingering of saline pore fluid can be observed
603 separating the freshwater interval at site M27. In the case of low anisotropy, this separation is
604 characterized by a relatively brackish zone. The simulated results indicate another freshwater
605 reservoir that extends oceanward of site M29. This reservoir has a sharp upper boundary that is
606 seaward dipping in correlation with the sedimentary bedding. The salinity gradually increases with
607 depth and distance offshore. This shallow body is preserved by near-surface low permeability
608 intervals. The most distal regions of the shelf models show complete salinization of all emplaced
609 freshwater. There is a broad region of fluid concentration that is just below ocean salinity.

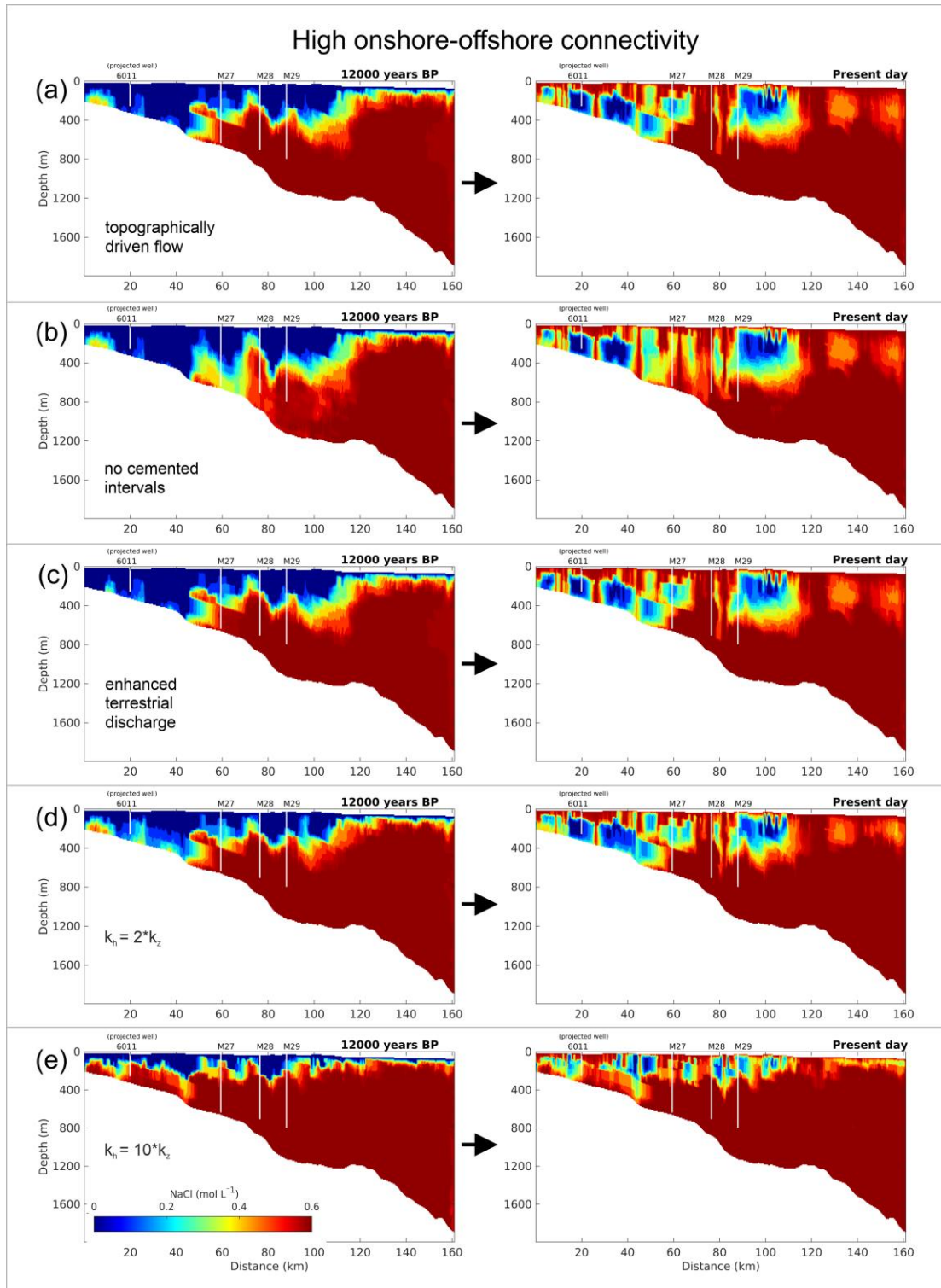
610

611 The numerical simulations with the high onshore-offshore connectivity model display similar
612 concentration distributions as described in the previous paragraph. The results are shown in Figure
613 15. In general, the proximal region of the shelf appears to undergo more freshening during the
614 recharge phase in all scenarios. Thick sand intervals in the HC model facilitate more advective
615 flushing with freshwater during the recharge phase. However, while the present day distributions
616 are broadly similar to the LC model, downward fingering of saline pore fluid results in more
617 compartmentalization of the seaward dipping fresh interval. Key differences are observed in the
618 the ETD scenario, where the proximal region of the model domain (0 km – 40 km) is completely
619 freshened during the recharge phase.



620
 621
 622
 623

Figure 14 Low onshore-offshore connectivity model showing pore fluid concentration at the end of the recharge phase (left) and present day (right) for simulated scenarios: (a) Base case, (b) cemented intervals, (c) enhanced terrestrial discharge, (d) - (e) anisotropic permeability.



624
 625 *Figure 15 High onshore-offshore connectivity model showing pore fluid concentration at the end of the recharge phase (left) and*
 626 *present day (right) for simulated scenarios: (a) Base case, (b) cemented intervals, (c) enhanced terrestrial discharge, (d) - (e)*
 627 *anisotropic permeability.*

628 Borehole pore fluid concentration profiles

629

630 Figure 16 shows the pore fluid concentration profiles extracted at the four well locations in both
631 model realizations. A close fit between simulated and measured data is observed at site 6011 in
632 both cases. All scenarios closely match the measured concentration with the exception of the high
633 anisotropic ratio. In the HC model, the profiles show lower concentrations compared to the LC
634 model, consistent with increased offshore directed flow of freshwater from the landward boundary.

635

636 At M27 there are two major freshwater intervals, an upper reservoir between 200 m – 400 m with
637 sharp boundaries, and a shallow interval characterized by a sharp upper boundary and gradually
638 increasing pore fluid concentration with depth. The upper reservoir is replicated with slightly
639 higher solute concentrations in both model realizations. In the case of high anisotropy and the
640 absence of cemented intervals, both models do not capture this upper reservoir. In the case of high
641 anisotropy, this reservoir is not freshened during the LGM (see Figure 14). In the absence of
642 cemented intervals we observe a salinization of the entire sediment column in the region of M27.
643 The lower reservoir is not reproduced in any of the modelled scenarios.

644

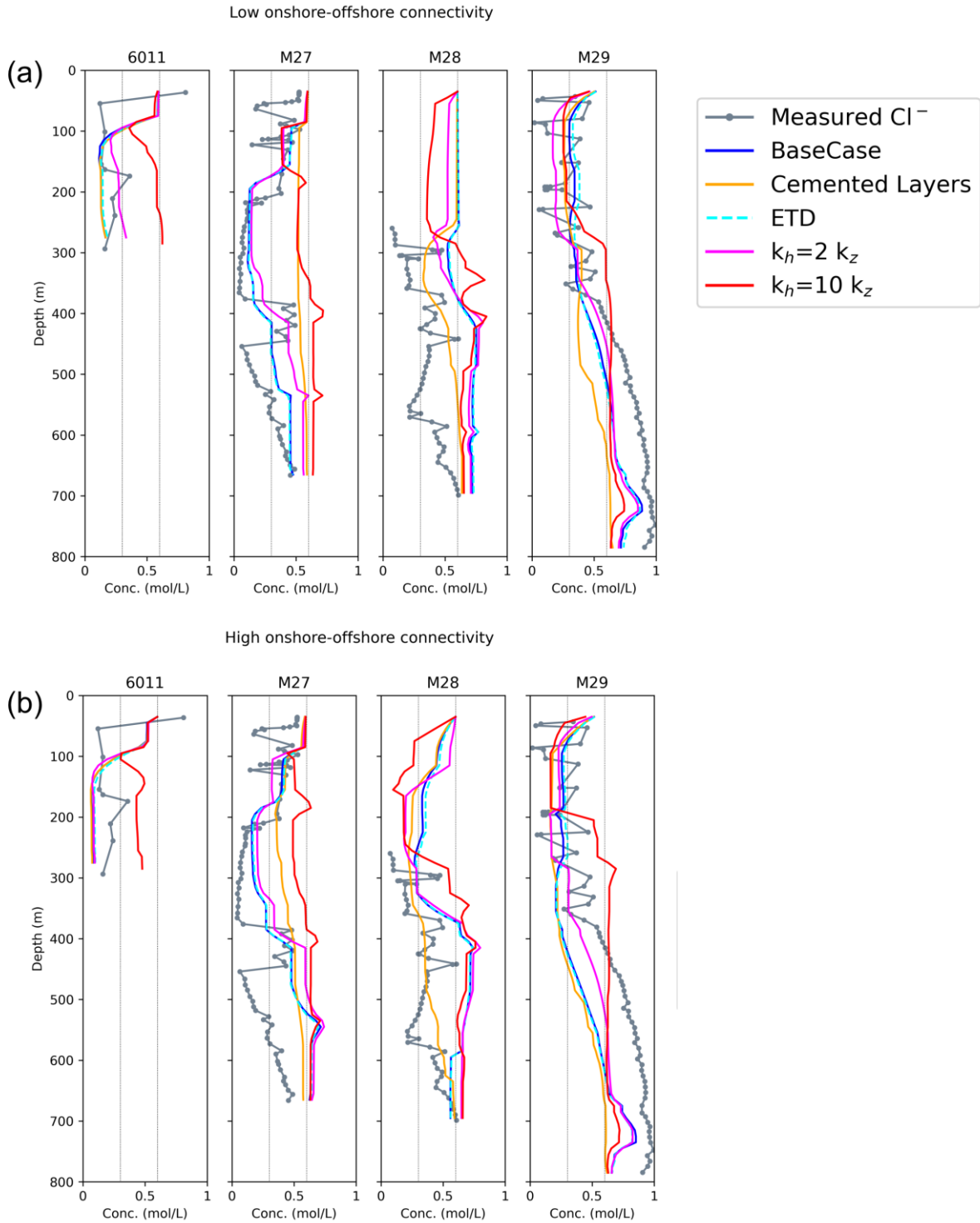
645 At well site M28, there is a stronger differentiation between the HC and LC models. The HC model
646 shows a fresh – brackish interval in the shallow part of the well (< 300 mbsf) in all scenarios,
647 which is consistent with the trend of the measured data. The LC model consistently over-estimates
648 the salinity in this region of the model. Given the close fit between the HC and LC models at the
649 more proximal M27, this misfit at M28 can be attributed to the differences in surface-connected
650 pathways in the two models rather than onshore-offshore connectivity (see Figure 12). The fresh –
651 brackish interval in the deeper section of the well is not reproduced exactly at the well location.
652 However, in the region around M28, both models show some brackish pore fluid down to ~500 m
653 (see Fig. 14).

654

655 The concentration profiles at site M29 closely match across all scenarios. The simulated results
656 generally represent the trend of the observed data, with a broad fresh – brackish zone in the upper
657 section of the well. The alternating fresh – saline intervals have been attributed to thin shale beds
658 on the centimetre scale (Mountain et al. 2010), which are below our model resolution. In the deeper

659 section of the well we observed some hyper-salinization of the pore fluid with a brine developing
 660 at ~700 mbsf.

661



662

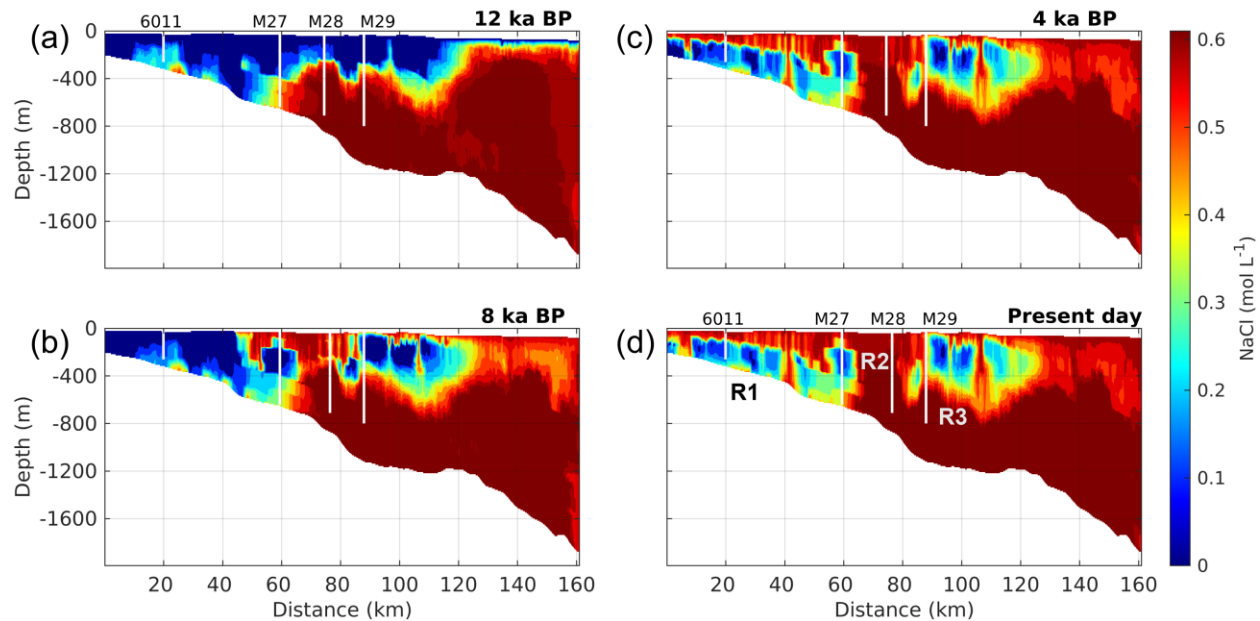
663 *Figure 16 Comparison between measured pore fluid concentration and simulated concentrations at 4 well locations in the model*

664 *domain. The low onshore-offshore connectivity model is shown in (a) and high onshore-offshore connectivity model.*

665 **3.1.3 Paleo-hydrological reconstruction on a representative shelf model**

666 This section presents the results of simulating conditions over the past 70 000 years until present
667 day, with a plausible combination of scenarios on a single representative model. Based on the
668 probability distribution of the suite of models (see Figure 5), we select the low onshore-offshore
669 connectivity model as the representative case.

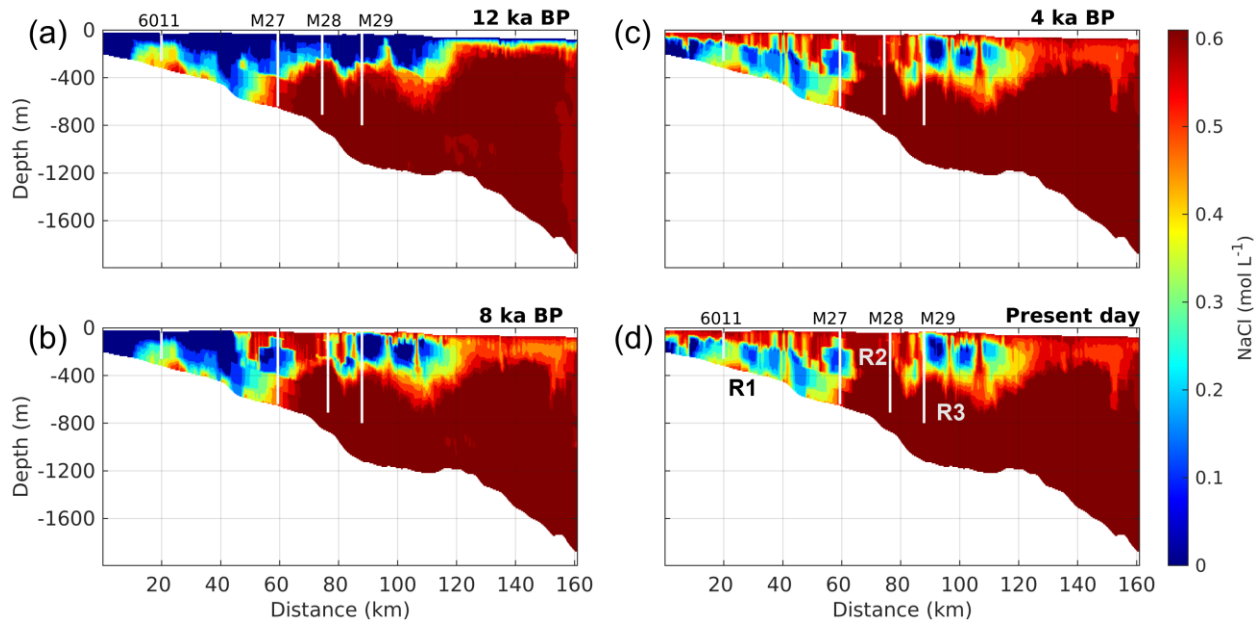
670 The transient simulation results are shown in Figure 17 for the isotropic permeability case. The
671 simulated present-day distribution shows a laterally extensive system of offshore freshened
672 groundwater with geometries correlating to the stratigraphic sequence boundaries on the shelf.
673 Surviving freshwater intervals are generally oceanward dipping with sharp upper boundaries.
674 Three main reservoirs can be identified in the present-day distribution (Figure 17 d). A thick interval
675 of freshwater extending from the landward boundary to about 40 km offshore (labelled R1). In the
676 region of site M27, a second freshwater reservoir is preserved by cemented and low-permeability
677 layers (labelled R2). Downward fingering of saline pore fluid around 40 km in the model domain
678 disconnects this reservoir from R1. Another laterally extensive zone of preserved freshwater
679 extends about 30 km oceanward from site M29 and becomes gradually more saline – R3. This
680 reservoir also appears to be compartmentalized by downward fingering saline pore fluid. The more
681 distal region is characterized by a relatively well mixed zone of pore fluid just below seawater
682 concentration.



683
 684 *Figure 17 Simulated pore fluid concentration on a geologically heterogeneous 2D model of the New Jersey shelf. Progressive*
 685 *salinization of emplaced groundwater is shown from the onset of the marine transgression 12 000 years ago (top left) to the present-*
 686 *day (bottom right). The surviving freshwater reservoir system is laterally extensive but compartmentalized by downward fingering*
 687 *of saline pore fluid via discontinuities in confining layers.*

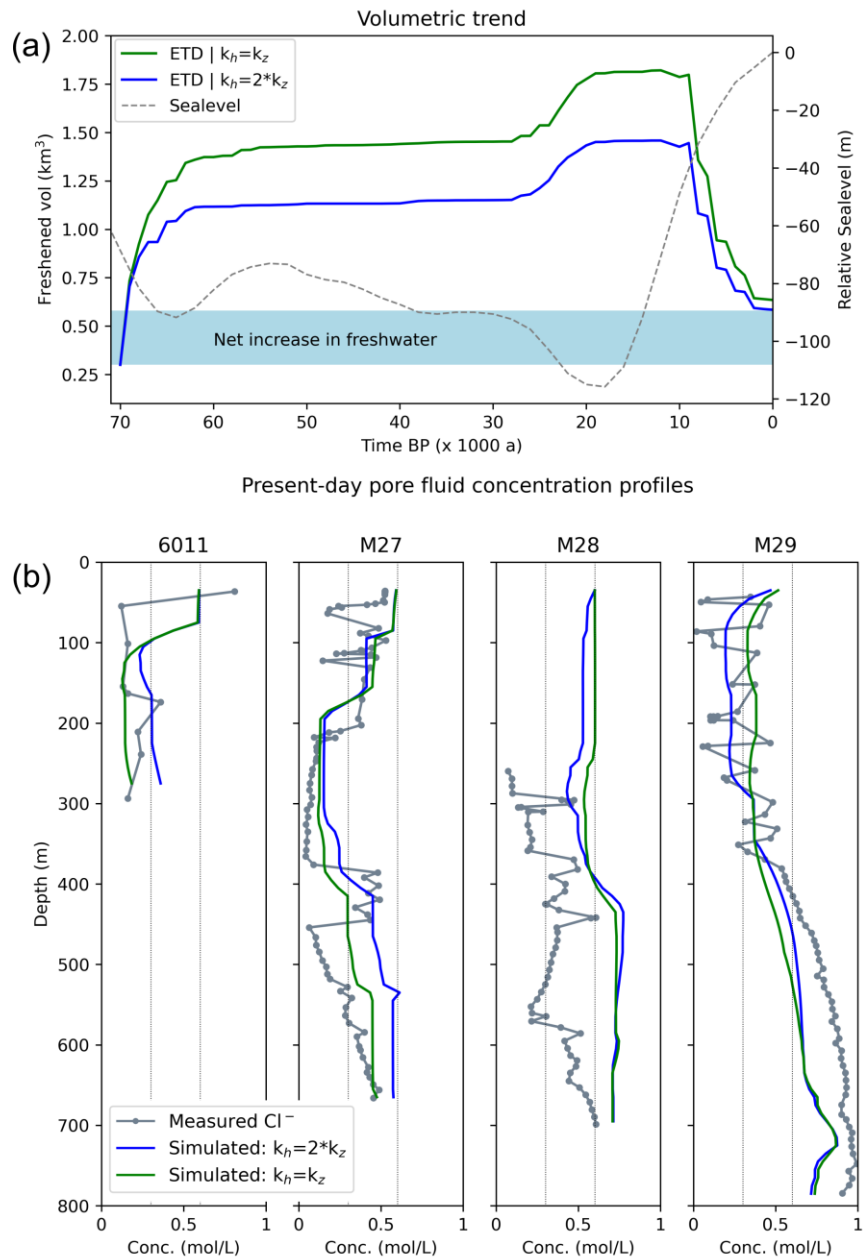
688 The results show that downward fingering of saline pore fluid during transgression occurs via
 689 seafloor-connected pathways. The denser fluid begins to diffuse laterally when low-permeability
 690 or cemented layers are encountered. This can lead to the observed alternating fresh and saline pore
 691 fluid intervals. The transient results of the transgressive period for the anisotropic permeability
 692 scenario ($k_h=2k_z$) are shown in Figure 18. The general observations are consistent with the isotropic

693 case. However, R1 and R2 are now separated by a zone of brackish pore fluid. The preserved
 694 intervals are marginally thinner in the presence of anisotropy.



695
 696 *Figure 18 Simulated pore fluid concentration on a geologically heterogeneous 2D model of the New Jersey shelf with anisotropic*
 697 *permeability where $k_x=2k_z$. Progressive salinization of emplaced groundwater is shown from the onset of the marine transgression*
 698 *12 000 years ago (top left) to the present (bottom right). The surviving freshwater reservoir system is laterally extensive but generally*
 699 *thinner than the isotropic permeability scenario.*

700 The volumetric trend shown in Figure 19 a, shows that although more freshwater recharge is
 701 emplaced during the isotropic permeability scenario, the surviving fresh water volumes are
 702 effectively the same. The system shows a net increase in the volume of freshwater that is stored
 703 over the regressive – transgressive cycle.



704

705 *Figure 19 Summary of key metrics for two simulated paleo-reconstructions: enhanced terrestrial discharge (ETD) with isotropic*
 706 *permeability (green), and ETD with $k_h=2*k_z$ (blue) (a) Freshwater volumetric curve for the paleo-reconstruction of the LGM on the*
 707 *representative 2D New Jersey shelf model. The shaded blue region shows the difference between the initial assumed volume of*
 708 *freshwater in the model domain and the present-day volume, highlighting the net increase in freshwater storage. (b) Comparison*
 709 *of measured and simulated concentration profiles at the borehole locations in the model domain. Blue curve shows the low-*
 710 *anisotropic permeability scenario, and the green curve shows the isotropic scenario.*

711 Simulated concentration profiles were compared to measured values at the well locations shown
 712 in Figure 19 b. At site 6011, both simulated profiles closely match the measured data. The freshwater
 713 preserved just below the seafloor in the measured data is not captured by the model. At site M27
 714 both scenarios reproduce the main freshwater interval (200 m – 400 m) with marginally higher

715 concentration. However, the deeper reservoir was not captured by the model. Once again, the
716 preserved freshwater just below the seafloor is not reproduced. At site M28, the models
717 underestimate the amount of freshwater stored in the sediment column. However, more freshwater
718 is preserved a few kilometres oceanward of this site. At site M29, the trend of the shallow multi-
719 layered freshwater system is broadly captured down to approximately 350 m. Below this depth,
720 the modelled salinities systematically underestimate the measured values, which might be
721 influenced by buried evaporites. However, some degree of hyper-salinization is observed.

722

723 **4 Discussion**

724 The simulation results provide detailed insight regarding the importance of geological
725 heterogeneity for the emplacement and subsequent preservation of freshwater into the sediments
726 of the New Jersey shelf. The numerical analysis provides strong evidence that the hydrogeologic
727 conditions on the shelf during the LGM, together with the sequence stratigraphic architecture can
728 lead to a complex layered OFG reservoir system. We employed a stochastic modelling approach
729 using the sequential indicator simulation (SIS) to populate the model domain with sand, silt and
730 shale facies. The variogram based approach is capable of sufficiently representing the sedimentary
731 patterns of the passive margin depositional setting on the shelf. That is a key consideration when
732 choosing a modelling approach (Seifert and Jensen 1999). An extended discussion on the
733 suitability of SIS for a 2D model of the New Jersey shelf is presented in Thomas et al. (2019).
734 Additionally, our approach incorporates geological information in the form of stratigraphic
735 boundaries interpreted on seismic data, and trends derived from borehole data. This has been
736 shown to reduce uncertainty in geostatistical models (Labourdette et al. 2008)

737 The Monte Carlo sampling of stochastic realizations allowed us to rank the models based on a key
738 system characteristic, i.e., onshore-offshore connectivity. This allows for the selection of
739 appropriate realizations from the probabilistic model. Analysis of dynamic response data is a
740 common way to reduce uncertainty in stochastic facies models as it carries information about flow
741 connectivity in the model domain (Hill and Tiedeman 2006). Each model realization honours the
742 available data and thus represents equally likely scenarios. It must be noted that the probability
743 distribution obtained is a function of the specific conditions assigned to the suite of models. The
744 conditions applied in this study were designed specifically to quantify the distribution of onshore-
745 offshore connectivity in the suite of models. This approach can be adapted in future studies to
746 investigate other components of OFG systems such as confining layer continuity.

747 **4.1 What drove freshwater emplacement on the New Jersey shelf?**

748 Our numerical study shows that periods of rapid sea-level fall during the LGM accelerated the
749 flushing of shelf sediments with freshwater via meteoric recharge. During the period of relatively
750 slow regression, the observed freshening trend is considerably flattened. The correlation between
751 rapid sea level fall and increased recharge was persistent across all simulated scenarios. All other

752 influences were superimposed on this trend. This observed dynamic supports the hypothesis that
753 sealevel fall drives vigorous freshwater flow toward the open ocean (Meisler et al. 1984). Previous
754 numerical studies of OFG systems have shown the influence of sealevel lowstand on freshwater
755 emplacement (Micallef et al. 2020; Person et al. 2003) . However, our results highlight the
756 particular influence of rapid rate of sea level fall. In general, the depth of freshwater recharge
757 increased inland with surface elevation. A 3D numerical study of the US mid-Atlantic shelf by
758 Siegel et al. (2014) highlighted the strong control of seafloor topography on fresh groundwater
759 emplacement. On average, observed salinities were lower in the relatively elevated eastern region
760 of their model over the simulated period. The New Jersey shelf has a gentle gradient, however it
761 is not consistently seaward sloping. Ocean floor bathymetry shows a slightly elevated region just
762 beyond the mid-shelf, 100 km from the coastline. This local topographic high corresponds to a
763 deeper circulation of freshwater during the low-stand period in all scenarios considered. This is
764 consistent with observations in a regional study by Siegel et al. (2014), where seafloor topography
765 was shown to be responsible for convection cells driving the re-distribution of fresh and saline
766 water to a depth of several hundred meters. In a study characterizing global offshore fresh
767 groundwater reservoirs, Zamrsky et al. (2020) showed that the topographic profile of the shelf is a
768 key characteristic governing the emplacement of freshwater in the system. These findings together
769 suggest that localized topographic variations on the seafloor should be considered as important
770 features, with a high likelihood to coincide with OFG in regions where the appropriate paleo-
771 hydrologic conditions existed.

772 The extent of freshwater recharge varies across the four well sites. The sediment column in the
773 most proximal part of the model near the projected location of well 6011 is completely freshened
774 in every scenario. Most of the sediment column in the region of M27 is freshened, with brackish
775 pore fluid remaining below 400 m in the well. The salinity distribution at the end of the recharge
776 phase indicate that freshening occurs by top-down as well as lateral flow of freshwater from the
777 landward direction. At site M28 and M29, freshening occurs down to a maximum of 300 m, the
778 deeper sediments remain relatively saline across all scenarios. Freshening in this region appears to
779 primarily occur by top-down meteoric recharge via surface-connected pathways. The model shows
780 that the LGM is not sufficient to freshen the deeper reservoirs that have been observed at sites M27
781 and M28. The deep freshwater intervals at those wells are either relics of a previous interglacial
782 period, or recharge via 3D flow pathways not captured in this study.

783 The offshore extent of freshening in our model is consistent with an earlier regional numerical
784 study of the Pleistocene glacial maximum on the US Atlantic margin by Cohen et al. (2010). That
785 study also reported freshwater emplacement at distances up to 100 km from the modern-day
786 coastline. They attributed this to offshore directed flow in shallow outcropping Miocene sands.
787 The layered regional model considered by Cohen et al. (2010) did not account for the presence of
788 discontinuities in confining layers. The lateral heterogeneity in our model captures this important
789 component of the recharge process, highlighting the importance of incorporating realistic
790 geological features when characterizing OFG systems. Recharge is not strictly confined to the
791 inland outcrops of sandy units, rather it occurs all across the shelf transect driven by the
792 topographic gradient and controlled by the sequence stratigraphic architecture. Our simulations
793 consider both low- and high onshore – offshore connectivity scenarios. These clearly show that
794 in the presence of geological heterogeneity, offshore-directed flow does not translate to increased
795 freshwater emplacement in the distal shelf region. This implies that offshore-directed flow, due to
796 terrestrial drivers such as over-pressure induced by ice-sheet loading, are not an absolute
797 requirement for emplacement of freshwater in sediments that are currently far offshore.

798 Previous numerical studies showed that increased advective forces which drive sub-glacial
799 freshwater emplacement do not extend far beyond the edge of the ice sheet (Cohen et al. 2010;
800 Siegel et al. 2014). Results obtained on this New Jersey transect of enhanced terrestrial discharge
801 are consistent with this dynamic system behavior. An elevated hydraulic head at the inland
802 boundary only affected the salinity observed in the proximal part of the model, while the overall
803 emplaced volume of freshwater increased only marginally in response to an increased hydraulic
804 head of 25 m at the inland boundary. This value was chosen to represent a high end member value
805 of enhanced terrestrial discharge based on regional reconstructions presented in Cohen et al.
806 (2010), which showed elevated heads of 30 m – 40 m during the Pleistocene lowstand in the region
807 onshore New Jersey shelf. This constant head value represents an estimate of potential offshore
808 directed flow. Actual values of offshore groundwater discharge are irregular and vary with time
809 (Burnett et al. 2006).

810 The most significant change in the volume of freshwater occurred when anisotropic permeability
811 was implemented. An anisotropic ratio of ten resulted in an observable change in the shape of the
812 freshwater – saltwater interface. These results suggests that the downward percolation of

813 freshwater into the sediment column via surface connected pathways is a crucial mechanism for
814 freshwater emplacement. Notably, the reduction in freshwater recharge was smaller in the HC
815 model. This we attribute to the higher lateral connectivity relative to the LC model, which allows
816 more freshwater into the sediments. However, in the case of higher anisotropy both models result
817 in similar volumes of recharge. This highlights again the importance of surface derived recharge.
818 Meisler et al. (1984) found that a lower anisotropy ratio resulted in a landward as well as downward
819 shift of the sharp interface position in their layered shelf model. This basic correlation is observed
820 in our results; however, the response is considerably more dynamic in the heterogeneous shelf
821 model. The implementation of a low anisotropy ratio of two, resulted in a closer fit to the observed
822 data. This suggests that the system can be characterized by low to moderate permeability
823 anisotropy. Our study highlights the importance of constraining permeability anisotropy in the
824 characterization of OFG systems. Anisotropy can be identified via specialized laboratory
825 measurements on core plugs (Crawford et al. 2008). Such an approach can improve model
826 constraints. However, upscaling to the field scale is a non-trivial part of incorporating this
827 information into flow models, which is dependent on the geological heterogeneity (Menke et al.
828 2021; Szymkiewicz 2013)

829 In the layered depositional setting of the New Jersey shelf, density instabilities occur as freshwater
830 is driven oceanward and advances non-uniformly. Preferential flow in high-permeability intervals
831 creates a complex combination of advective and diffusive processes during the lowstand period.
832 We found two key mechanisms of freshening. The primary mechanism is advective freshening
833 driven by the oceanward hydraulic gradient. This causes freshwater to flow preferentially into
834 high-permeability sediment layers, flushing out the salt water. Density instabilities occur where
835 aquifer units are freshened while overlying confining units remain saturated with denser saline
836 pore fluid for a longer period. In the early stages of recharge, this juxtaposition results in sharp
837 salinity contrasts between aquifers and overlying confining units. This contrast gives way to the
838 secondary mechanism, convective mixing, resulting from the unstable concentration gradients in
839 the layered sedimentary setting. Denser saline pore fluid in confining layers fingers downward into
840 freshened intervals, while more buoyant freshwater migrates upward. The temperature gradient on
841 the shelf likely contributes to the buoyancy of freshwater driven deeper into the sediment column.

842 **4.2 Marine transgression and freshwater survival**

843 Kooi et al. (2000) conducted a numerical study analyzing the various modes by which seawater
844 intrusion occurs during a marine transgression. Their study identified four modes: (1) horizontal
845 intrusion in the case of a slow transgression, (2) vertical intrusion by seawater fingering during
846 rapid transgression over a highly permeable medium, (3) vertical intrusion by diffusion for rapid
847 transgressions over a low-permeability medium, and (4) vertical intrusion by a combination of
848 diffusion and low-salinity fingering for rapid transgression over a layered subsurface. Kooi et al.
849 (2000) showed that there is a critical rate of marine transgression that determines whether a
850 transition occurs from horizontal to one of the vertical intrusion modes. The marine transgression
851 that took place after the last glacial maximum can be considered as above critical for the low-angle
852 New Jersey shelf. The 161 km model domain proceeded from sub-aerial exposure to complete
853 inundation with ocean water in approximately 12 000 years from the LGM to the present day. This
854 corresponds to a transgression rate of approximately 13 m per year. Based on the results obtained
855 in this study, there is evidence for three vertical modes of intrusion associated with the rapid
856 transgression. In the distal region of the shelf, where low-permeability facies are dominant, a
857 seaward dipping wedge of low-salinity pore fluid develops during the transgression. In the mid-
858 shelf region, low-permeability intervals near the ocean floor preserve a substantial amount of fresh
859 water, however, downward fingering of saline fluid through overlying shales create lateral salinity
860 variations in the reservoir (R3). This results in a broad and relatively well-mixed transition zone
861 on the oceanward end of this reservoir. The landward part of R3 is characterized by sharp
862 boundaries between freshwater intervals and saline pore fluid in overlying confining layers (see
863 Fig. 17). In the more proximal region of the shelf, the permeability distribution trends towards
864 more high-permeability sands, where a different mode can be observed. This mode is characterized
865 by downward fingering ocean water creating a high-salinity pore fluid columns, which
866 compartmentalize the surviving freshwater body (Fig. 17 and 18). A field study of vertical
867 seawater intrusion on a freshwater lens by Post and Houben (2017) showed that downward
868 fingering of saline pore fluid was the dominant driver of mixing. Groen et al. (2000) showed how
869 this downward fingering process can speed up the salinization of sequestered freshwater on the
870 continental shelf. Our stochastic New Jersey shelf model accounts for discontinuities in the
871 overlying confining units, and thus highlights the importance of geological heterogeneity on the
872 survival of offshore freshened groundwater. Future numerical studies, for example in 3D, can

873 benefit from considering the various modes of intrusion that generated by the subsurface
874 heterogeneity and underlying regional permeability trends. The 2D approach presented in this
875 study does not account for all potential flow pathways.

876 The present-day scenario consisting of a layered and compartmentalized fresh-brackish water zone
877 results from connected pathways between the ocean and deeper, permeable sediments. Along these
878 pathways, density-driven flow salinifies most permeable units, while cemented and low-
879 permeability intervals shield some freshwater reservoirs from above. These findings support the
880 salinification mechanisms suggested by Lofi et al. (2013) for mid-shelf reservoirs based on a
881 qualitative shelf model. These authors postulated that either outcropping reservoirs at the seafloor,
882 or a pathway of intermediary connected reservoirs could explain the salinization of the mid-shelf
883 region. Our numerical simulations favor the latter of these two explanations. Lateral heterogeneity
884 results in complex, connected pathways between the ocean and deeper reservoirs of emplaced
885 freshwater. This is consistent with earlier simulations of surviving freshwater body in a
886 heterogeneous shelf model presented by Thomas et al. (2019), in which authors showed that the
887 observed salinity distribution is strongly influenced by the stratigraphic architecture. As we
888 address this problem only in 2D, the full complexity and influence of such pathways cannot be
889 entirely captured. In a 3D model, ocean water can enter reservoirs from multiple directions,
890 resulting in different survival rates for freshened reservoirs. However, considering that
891 depositional environment for Miocene sediments has been identified as wave-dominated
892 (Monteverde et al. 2008; Proust et al. 2018), we postulate that the complexity of the groundwater
893 flow and solute transport on New Jersey shelf is largely a function of dip-oriented variation in
894 sediment properties. Based on the principles of a wave-dominated environment, it can be assumed
895 that there is considerably less variation in sediment properties in the shoreline parallel direction.
896 The 2D model thus provides a representative perspective on the dynamic life cycle of offshore
897 freshened groundwater in the New Jersey passive margin setting.

898 **4.3 Modern or Fossil Water?**

899 The results of our numerical study can be discussed in the light of the two main hypotheses
900 proposed for explaining the presence of freshwater offshore New Jersey. The first hypothesis
901 identifies the source as meteoric and sub-ice-sheet recharge during the sea-level lowstand

902 associated with the last glacial maximum or potentially earlier periods (Cohen et al. 2010; Kooi
903 and Groen 2001; Person et al. 2003; Siegel et al. 2014). Results presented in this study show that
904 both high- and low-permeability sediments of the New Jersey shelf were flushed with freshwater
905 during the LGM in all scenarios considered. At the expedition 313 well sites in the mid-shelf
906 region, we observed freshening of the shallow reservoirs, consistent with present-day observations.
907 However, deeper reservoirs in M27 and M28 remained relatively saline during the simulated
908 period. In the subsequent transgressive period, these reservoirs underwent partial salinification,
909 but a significant portion of fresh – brackish water survives to the present day. This observation
910 supports the hypothesis that freshwater sampled at Expedition 313 sites would be fossil water
911 emplaced via meteoric recharge during the LGM. Our simulations suggest that the deeper
912 reservoirs in M27 and M28 may even pre-date the LGM. An alternative explanation for these
913 reservoirs is that they were recharged via shoreline parallel connected flow pathways, which our
914 2D model does not capture. It is plausible that a full 3D characterization of the shelf would result
915 in the freshening of these deeper reservoirs during the LGM.

916 To date there have been no published studies on the absolute ages of groundwater sampled at the
917 Expedition 313 sites. In an earlier coastal aquifer study, McAuley et al. (2001) analysed radioactive
918 isotopes in four wells in order to estimate groundwater ages in the coastal Atlantic City 800-foot
919 sand, the principal source of water supply for southern New Jersey coastal communities. Their
920 transect extended from inland to approximately 8.5 km offshore. At the Pleasantville well site, 1.6
921 km inland of the coastline, sampled water was dated at 17 950 years BP. The two offshore sites
922 yielded ages of at least 22 000 years BP and possibly older than 30 000 years BP. These dates
923 support the hypothesis of Pleistocene freshwater emplaced in the mid-shelf reservoirs. As a caveat,
924 van Geldern et al. (2013) reasoned that these dates may be over-estimated, as it cannot be verified
925 whether the relevant correction models were used in the calculation of the radiocarbon ages.

926 Despite not providing information on absolute ages, stable isotope ratios of oxygen and hydrogen
927 in water were used as natural tracers to characterize the origins and composition in both marine
928 and terrestrial studies (Bigg and Rohling 2000; Bowen and Wilkinson 2002; Dutton et al. 2005;
929 Maslin and Swann 2006). van Geldern et al. (2013) analysed the stable isotope composition of
930 Expedition 313 samples. They concluded that the freshwater was either of modern meteoric origin
931 and therefore rapidly recharged, or it pre-dates the Pleistocene and had been recharged during a

932 period with similar climatic conditions to modern times. $\delta^{18}O$ values of water sampled at
933 Expedition 313 sites range between -0.8 ‰ and -7.0 ‰, indicating a mixture of modern meteoric
934 recharge and seawater as the source of pore fluids (van Geldern et al. 2013). Water of Pleistocene
935 age would normally be characterized by a comparatively lower range of isotope values (Mook and
936 Rozanski 2000): $\delta^{18}O$ values in the range of -11 ‰ to -18.0 ‰ were reported for Pleistocene-age
937 recharge in the Cambrian-Ordovician aquifer of Iowa, further inland on the North American
938 continent (Siegel 1991). However, an isotopically depleted body of Pleistocene water was shown
939 there to be caused by a dilution of a combination of glacial meltwater and precipitation. This
940 diluted water mass was deep in the aquifer, below 300 m of confining layers, and $\delta^{18}O$ values are
941 within the range of modern precipitation for Iowa (from -11 to -6.0 ‰) (Siegel 1991). This
942 regional setting of the sample locations analysed by Siegel (1991., Fig. 2) is analogous to the New
943 Jersey case, which had not been covered by ice-sheets as it was rather proximal to the edges of
944 their southern-most advance (Cohen et al. 2010). The depleted isotopic signature of the Pleistocene
945 groundwater suggests that the climate at the end of the last glacial period was mild. This conclusion
946 is also supported in multi-disciplinary studies (Hanshaw et al. 1979; Morgan et al. 1987). These
947 studies provide strong evidence that groundwater isotope values similar to that of modern
948 precipitation do not unambiguously indicate recent recharge.

949 Our simulation results do not support any significant role of modern recharge in the persistence of
950 the mid-shelf freshwater system observed by IODP Expedition 313 (Mountain et al. 2010).
951 Previous studies have shown that in certain geological settings, an active recharge of offshore
952 freshened groundwater reservoirs can occur (Michael et al. 2016; Varma and Michael 2012). Our
953 stochastic approach considered both high and low onshore-offshore connectivity scenarios and
954 found only marginal changes in present-day freshwater distributions at the most proximal regions
955 of the model domain (i.e., well site 6011). Observed profiles at IODP expedition 313 sites are
956 unaffected by offshore directed discharge. A more speculative hypothesis suggests that the
957 freshwater may date back to the Miocene age (Meisler et al. 1984). In a study of groundwater
958 residence times in the Alberta Basin Gupta et al. (2015) performed simulations constrained by
959 hydrogeologic and geochemical observations. The results showed dilution of old pore fluids
960 occurred due to flushing by younger waters. The hydrogeologic model presented in this New
961 Jersey study shows that significant flushing of the mid-Miocene sediments likely occurred during

962 the last glacial maximum. This exchange and mixing of pore fluid likely occurred in multiple
963 glacial – interglacial cycles and can therefore influence the age of pore fluid determined solely by
964 geochemical methods. Our numerical results strongly suggests that water emplaced before the
965 Pleistocene would have likely been flushed out since, and consequently, its signature would have
966 been over-printed by relatively younger groundwater, as speculated by Meisler et al. (1984).

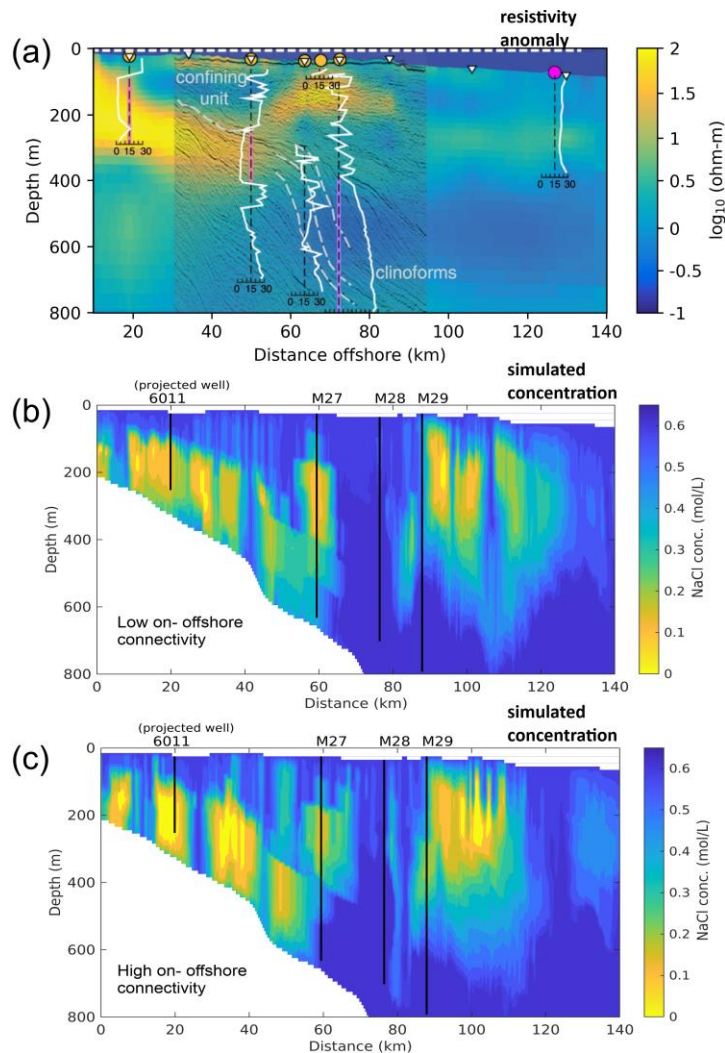
967

968 The results of this study are broadly consistent with the salinity profiles of the multi-layered
969 reservoir system of offshore freshened groundwater observed in IODP Expedition 313 (Mountain
970 et al. 2010) and the projected position of AMCOR well site 6011. Portions of the surviving
971 freshwater in our numerical simulations are also consistent with the resistivity anomalies identified
972 by an independently conducted electromagnetic survey of the US continental shelf by Gustafson
973 et al. (2019). In the proximal region of the shelf, Gustafson et al. (2019) considered the strong
974 resistivity anomaly as evidence for an active connection between onshore and offshore freshwater
975 reservoirs. However, numerical simulations show that offshore directed only influences the
976 freshwater in the most proximal region of the model (i.e., within 20 km from the landward
977 boundary). Downward fingering ocean water compartmentalizes the surviving freshwater system
978 into isolated, hydraulically disconnected pockets as discussed earlier. In both high and low
979 onshore-offshore connectivity scenarios, the offshore directed discharge is insufficient to maintain
980 open freshwater conduits to the surviving reservoirs in the mid-shelf region. Figure 20 shows a
981 visual comparison between the resistivity anomaly and our paleo-reconstruction on both high and
982 low connectivity model scenarios. Our model domain was clipped, and color scales were adjusted
983 to match the presented resistivity data. There is a reasonably close fit between the resistivity
984 anomalies and the simulated freshwater distribution. The proximal body of freshwater preserved
985 in our model is consistent with the seaward dipping resistivity anomaly presented by Gustafson et
986 al. (2019). However, our heterogeneous model domain captures lateral variability in pore fluid
987 concentration resulting from downward fingering via seafloor-connected pathways. This
988 downward fingering is more pronounced in the high onshore-offshore connectivity model, as it
989 features thicker high permeability intervals that more readily facilitate downward fingering. A
990 numerical study of aquifer vulnerability to ocean storm surges by Cardenas et al. (2015) found that
991 while zones of downward fingering saline pore fluid were apparent in their numerical model
992 results, there was only tentative evidence of their existence in the geophysical field measurements.

993 Electromagnetic methods integrate resistivity over volumes which become larger with increasing
994 depth. Therefore, small-scale signatures at greater depth, such as the saline fingers are not resolved.
995 Finally, the shallow anomaly in the mid-shelf region, which gradually fades in the oceanward
996 direction is similar to the preserved freshwater reservoir earlier described as R3. This reservoir has
997 the lowest salinity in the region of M29 and gradually becomes more saline in the oceanward
998 direction, consistent with the trend of the anomaly.

999

1000 Figure 20 shows a qualitative comparison between independent datasets. Future studies can benefit
1001 from integrating numerical flow simulations into a process-based inversion scheme to improve
1002 constraints of subsurface properties such as hydraulic conductivity or porosity (Wagner and
1003 Uhlemann 2021). A stochastic approach to capture geological heterogeneity, as presented in this
1004 paper, can produce more geologically representative constraints on porosity distribution, which
1005 strongly influences the interpretation of resistivity data. Additionally, structurally constrained
1006 inversion can integrate known stratigraphic features, such as cemented intervals, into geophysical
1007 data processing as detailed by Wagner and Uhlemann (2021).



1008

1009 *Figure 20 Visual comparison of resistivity anomaly report by Gustafson et al. (2019) and numerical simulation results of our paleo-*
 1010 *hydrological reconstruction of the LGM on the New Jersey shelf. (b) and (c) show the low and high onshore – offshore connectivity*
 1011 *scenarios, respectively. Both results show freshwater distribution that is broadly consistent with the observed resistivity anomaly.*
 1012 *Future studies can benefit from joint or process based inversion of resistivity data to better constrain the characterization of OFG*
 1013 *systems.*

1014 Based on the evidence of this numerical study, and previous findings discussed earlier, we
 1015 conclude that the freshwater system had been almost completely recharged during the lowstand
 1016 period associated with the last glacial maximum beginning at least 70 000 years ago. Although not
 1017 studied here, it can also be safely assumed that some partial recharge into the sediments also
 1018 occurred prior to 70 000 years ago. Therefore, the observed freshwater system is slowly shrinking
 1019 due to diffusion and density-driven flow through connected pathways to the ocean. This
 1020 observation does not account for the 3D effects of laterally connected pathways that can likely
 1021 alter the observed distribution. The net increase in freshwater stored on the New Jersey shelf over
 1022 the simulated period suggest that the cyclical flushing and re-salinization of shelf sediments, which

1023 takes place over glacial – interglacial cycles is an asymmetrical process. This means that some
1024 portion of the freshwater recharged into the system during glacial sea-level lowstands will likely
1025 survive the typical inter-glacial period and thus the system favours storage of freshened pore fluid
1026 over geological time-scales. A numerical study of freshwater survival on the New Jersey shelf by
1027 Thomas et al. (2019) also found that at least 15 % of initially assumed freshwater volume had
1028 survived after simulating 30 000 years of ocean coverage.

1029 **4.4 Resource perspective**

1030 We present some simple back-of-the-envelope calculations based on the paleo-reconstruction
1031 presented in this study. The volume of freshwater in this case was approximately 0.54 km^3 . The
1032 model cell width of 100 m means this can be expressed as a potential storage of 5.4 km^3 of fresh-
1033 to-brackish water per kilometer of the New Jersey coastline. This is more than a previous estimate
1034 of 3.8 km^3 of freshened groundwater per kilometer of coastline presented in a study by Cohen et
1035 al. (2010), which was an average value based on data from four different continental shelf
1036 transects. The value presented by Cohen et al. (2010) is based on an effective sediment porosity of
1037 20 %. The estimate presented in this study is directly related to the New Jersey case of relatively
1038 unconsolidated sediments on a passive margin setting, with porosity ranging from 40 % to 60 %.
1039 Extrapolating these results along 180 km of the New Jersey coastline, we estimate about 1 000
1040 km^3 of fresh to brackish water to exist under present-day conditions on the shelf. A comparable
1041 value of 1 300 km^3 of freshwater was estimated to be sequestered in continental shelf reservoirs in
1042 New England, US (Cohen et al. 2010). To put this into perspective, the daily groundwater water
1043 extraction in entire United States, was estimated at 73 km^3 in 2010 , based on an extraction rate of
1044 $0.2 \text{ km}^3 / \text{day}$ (Maupin et al. 2014).

1045 The New Jersey shelf is only one of several occurrences of extensive systems of offshore
1046 freshened groundwater (Micallef et al. 2020a). As the understanding of these systems continues to
1047 expand, an important next step is the characterization of offshore fresh groundwater reservoirs.
1048 The results of this study on a representative geological model highlight the complex and dynamic
1049 interplay of topography, sediment heterogeneity, and anisotropy of permeability. These factors
1050 appear to have systemic effects on the volume of freshwater emplaced during low-stand periods
1051 as well as the survival and storage of this freshwater during subsequent transgressive periods. The

1052 characterization of offshore freshened groundwater requires dedicated hydrogeological data
1053 acquisition and analysis for deciphering the complex history of these reserves and characterizing
1054 their resource potential.

1055 **5 Conclusions**

1056 Integrating realistic heterogeneity based on seismic and well data can explain the multi-layered
1057 freshwater system on the New Jersey shelf. A geologically representative model shows that the
1058 OFG system is laterally compartmentalized by downward fingering saline fluids through
1059 connected pathways to the ocean. This shows that the accurate modelling of offshore fresh
1060 groundwater reservoirs requires adequate characterization of the geological heterogeneity. Our
1061 sensitivity analysis shows surface derived meteoric recharge is the primary mechanism for
1062 freshening of the sediment column during sealevel lowstand. Surface connected pathways and
1063 permeability anisotropy are therefore fundamental characteristics of the New Jersey shelf OFG
1064 system.

1065 By using a stochastic modeling approach to generate high and low onshore-offshore connectivity
1066 scenarios, we show that terrestrial discharge is not responsible for the freshwater intervals
1067 observed at Expeditions 313 well sites. Meteoric recharge during the lowstand associated with the
1068 LGM can sufficiently explain the existence of shallow reservoirs (< 400 mbsf). The emplacement
1069 of freshwater was driven primarily by the topographic gradient, which caused surface recharge to
1070 infiltrate the oceanward-dipping sediments. Deeper freshened intervals at wells sites M27 and M28
1071 are either relics of a previous interglacial period, or were recharged via 3D flow pathways not
1072 captured in this study. However, the increasing salinity with depth is not consistent with a deeper
1073 freshwater source.

1074 Finally, the observed volumetric trends suggest that the cyclical flushing and re-salinization of
1075 shelf sediments that takes place over glacial – interglacial cycles is an asymmetrical process, which
1076 favours storage of freshened pore fluid. In light of present-day stressed water supply and changing
1077 climate conditions, this has implications for the consideration of these unconventional
1078 groundwater resources. While our estimates of the freshwater volume stored on the New Jersey
1079 shelf qualifies them as a potential resource, it is important to note that these reserves are stored in
1080 low-permeability intervals and are slowly shrinking due to salinization.

1081 **Acknowledgments and Data**

1082 Simulations were performed with computing resources granted by RWTH Aachen University
1083 under project rwth0761.

1084 Funding for this project is provided by the Deutsche Forschungsgemeinschaft (DFG) within the
1085 Priority Programme 527 – “International Ocean Discovery Program” (IODP) under grant RE-
1086 3863/2-

1087 Directions to access to the algorithm used to generate the results in this study (SHEMAT-Suite) is
1088 available in the in-text data citation reference: Keller et al. (2020). This software is open source.

1089 **References**

1090 Austin J. A., Christie-Blick N., Malone M. J. (1998) Proc. ODP, Init. Rpts, 174A, College Station,
1091 TX (Ocean Drilling Program), doi: 10.2973/odp.proc.ir.174a.1998.

1092 Bigg G. R., Rohling E. J. (2000) An oxygen isotope data set for marine waters, *Journal of*
1093 *Geophysical Research* 105(C4):8527–8535.

1094 Bowen G. J., Wilkinson B. (2002) Spatial distribution of $\delta^{18}\text{O}$ in meteoric precipitation, *Geology*
1095 30(4):315, doi: 10.1130/0091-7613(2002)030<0315:SDOOIM>2.0.CO;2.

1096 Burnett W. C., Aggarwal P. K., Aureli A., Bokuniewicz H., Cable J. E., Charette M. A., Kontar
1097 E., Krupa S. et al. (2006) Quantifying submarine groundwater discharge in the coastal zone
1098 via multiple methods, *The Science of the total environment* 367(2-3):498–543, doi:
1099 10.1016/j.scitotenv.2006.05.009.

1100 Cardenas M. B., Bennett P. C., Zamora P. B., Befus K. M., Rodolfo R. S., Cabria H. B., Lapus M.
1101 R. (2015) Devastation of aquifers from tsunami-like storm surge by Supertyphoon Haiyan,
1102 *Geophysical Research Letters* 42(8):2844–2851, doi: 10.1002/2015GL063418.

1103 Clauser C (2003) Numerical simulation of reactive flow in hot aquifers using SHEMAT and
1104 Processing SHEMAT. Springer, Berlin.

- 1105 Cohen D., Person M., Wang P., Gable C. W., Hutchinson D., Marksamer A., Dugan B., Kooi H.
1106 et al. (2010) Origin and extent of fresh paleowaters on the Atlantic continental shelf, USA,
1107 *Groundwater* 48(1):143–158.
- 1108 Crawford B. R., Webb D. W., Searles K. H. (2008) Plastic Compaction and Anisotropic
1109 Permeability Development in Unconsolidated Sands with Implications for Horizontal Well
1110 Performance. In *The 42nd U.S. Rock Mechanics Symposium (USRMS)*. American Rock
1111 Mechanics Association, San Francisco, California.
- 1112 Deutsch CV, Pyrcz M (2014) *Geostatistical reservoir modeling*. Second edition / Michael J. Pyrcz,
1113 Clayton V. Deutsch. Oxford University Press, Oxford.
- 1114 Dutton A., Wilkinson B. H., Welker J. M., Bowen G. J., Lohmann K. C. (2005) Spatial distribution
1115 and seasonal variation in $\delta^{18}O$ / $\delta^{16}O$ of modern precipitation and river water across the
1116 conterminous USA, *Hydrological Processes* 19(20):4121–4146, doi: 10.1002/hyp.5876.
- 1117 Freeze RA, Cherry JA (1979) *Groundwater*. Prentice Hall, Englewood Cliffs, NJ.
- 1118 Gelhar L. W., Welty C., Rehfeldt K. R. (1992) A critical review of data on field-scale dispersion
1119 in aquifers, *Water Resources Research* 28(7):1955–1974, doi: 10.1029/92WR00607.
- 1120 Groen J., Velstra J., Meesters A.G.C.A. (2000) Salinization processes in paleowaters in coastal
1121 sediments of Suriname: evidence from $\delta^{37}Cl$ analysis and diffusion modelling,
1122 *Journal of Hydrology* 234(1-2):1–20, doi: 10.1016/S0022-1694(00)00235-3.
- 1123 Gupta I., Wilson A. M., Rostron B. J. (2015) Groundwater age, brine migration, and large-scale
1124 solute transport in the Alberta Basin, Canada, *Geofluids* 15(4):608–620, doi:
1125 10.1111/gfl.12131.
- 1126 Gustafson C., Key K., Evans R. L. (2019) Aquifer systems extending far offshore on the U.S.
1127 Atlantic margin, *Scientific reports* 9(1):8709, doi: 10.1038/s41598-019-44611-7.
- 1128 Hampson G. J. (2010) Sediment dispersal and quantitative stratigraphic architecture across an
1129 ancient shelf, *Sedimentology* 57(1):96–141, doi: 10.1111/j.1365-3091.2009.01093.x.

- 1130 Hanshaw B. B., Winograd I. J., Pearson F. J., Jacoby G. C. (1979) Stable isotope studies of
1131 subglacially precipitated carbonates and of ancient ground water: Paleoclimatic
1132 implications. In Gordon Jacoby (ed.) *Proceedings of International Meeting on Stable*
1133 *Isotopes in Tree-Ring Research*. Lamont-Doherty, Geological Observatory, Columbia
1134 University New York, New Paltz, New York:102–104.
- 1135 Hastie T, Tibshirani R, Friedman JH (2009) *The elements of statistical learning* Data mining,
1136 inference, and prediction / Trevor Hastie, Robert Tibshirani, Jerome Friedman. 2nd ed.
1137 Springer, New York (Springer series in statistics).
- 1138 Hathaway J. C., Poag C. W., Valent P. C., Miller R. E., Schultz D. M., Manhe F. T., Kohout F. A.,
1139 Bothner M. H. et al. (1979) US Geological Survey Core Drilling on the Atlantic Shelf,
1140 *Science* 206(4418):515–527.
- 1141 Hill MC, Tiedeman CR (2006) *Effective Groundwater Model Calibration With Analysis of Data,*
1142 *Sensitivities, Predictions, and Uncertainty*. John Wiley & Sons.
- 1143 Hobbs B., Ord A. (2015) Fluid Flow. In BE Hobbs, Ord, Alison (eds.) *Structural geology. The*
1144 *Mechanics of Deforming Metamorphic Rocks*. Elsevier, Amsterdam, Netherlands:365–
1145 421.
- 1146 Holcomb D. J., Olsson W. A. (2003) Compaction localization and fluid flow, *Journal of*
1147 *Geophysical Research* 108(B6), doi: 10.1029/2001JB000813.
- 1148 Imbrie J., Hays J. D., Martinson D. G., McIntyre A., Mix A. C., Morley J. J., Pisias N. G., Prell
1149 W. L. et al. (1984) The orbital theory of Pleistocene climate: support from a revised
1150 chronology of the marine d18O record. In A Berger (ed.) *Milankovitch and Climate, Part*
1151 *1*. D. Reidel Publishing Company, Boston, MA.
- 1152 Jazayeri A., Werner A. D. (2019) Boundary Condition Nomenclature Confusion in Groundwater
1153 Flow Modeling, *Ground Water* 57(5):664–668, doi: 10.1111/gwat.12893.
- 1154 Johnsen S. J., Dahl-Jensen D., Dansgaard W., Gundestrup N. (1995) Greenland
1155 palaeotemperatures derived from GRIP bore hole temperature and ice core isotope profiles,
1156 *Tellus B* 47(5):624–629, doi: 10.1034/j.1600-0889.47.issue5.9.x.

- 1157 Johnston R. H. (1983) The saltwater-freshwater interface in the Tertiary limestone aquifer,
1158 southeast Atlantic outer-continental shelf of the U.S.A, *Journal of Hydrology* 61(1-3):239–
1159 249, doi: 10.1016/0022-1694(83)90251-2.
- 1160 Keller J., Rath V., Bruckmann J., Mottaghy D., Clauser C., Wolf A., Seidler R., Bücker H. M. et
1161 al. (2020) SHEMAT-Suite: An open-source code for simulating flow, heat and species
1162 transport in porous media, *SoftwareX* 12:100533, doi: 10.1016/j.softx.2020.100533.
- 1163 Kooi H., Groen J. (2001) Offshore continuation of coastal groundwater systems; predictions using
1164 sharp-interface approximations and variable-density flow modelling, *Journal of Hydrology*
1165 246(1):19–35.
- 1166 Kooi H., Groen J., Leijnse A. (2000) Modes of seawater intrusion during transgressions, *Water*
1167 *Resources Research* 36(12):3581–3589, doi: 10.1029/2000WR900243.
- 1168 Labourdette R., Hegre J., Imbert P., Insalaco E. (2008) Reservoir-scale 3D sedimentary modelling:
1169 approaches to integrate sedimentology into a reservoir characterization workflow,
1170 Geological Society, London, Special Publications 309(1):75–85, doi: 10.1144/SP309.6.
- 1171 Lachenbruch A., Sass J. H. (1977) Heat flow from the crust of the United States and the Thermal
1172 Regime of the Crust. In Heacock JG, Keller GV, Oliver JE, Simmons G (eds.) *The Earth's*
1173 *Crust*, vol. 20. American Geophysical Union, Washington:p 635–675.
- 1174 Lofi J., Inwood J., Proust J.-N., Monteverde D. H., Loggia D., Basile C., Otsuka H., Hayashi T. et
1175 al. (2013) Fresh-water and salt-water distribution in passive margin sediments: Insights
1176 from Integrated Ocean Drilling Program Expedition 313 on the New Jersey Margin,
1177 *Geosphere* 9(4):1009–1024.
- 1178 Malone M. J., Claypool G., Martin J. B., Dickens G. R. (2002) Variable methane fluxes in shallow
1179 marine systems over geologic time: The composition and origin of pore waters and
1180 authigenic carbonates on the New Jersey shelf, *Marine Geology* 189(3):175–196.
- 1181 Manahan SE (2011) *Fundamentals of Environmental Chemistry*, Third Edition. CRC Press.

- 1182 Maslin M. A., Swann G. E.A. (2006) Isotopes in Marine Sediments. In MJ Leng (ed.)Isotopes in
1183 Palaeoenvironmental Research. Developments in paleoenvironmental research, vol. 10.
1184 Springer, Dordrecht.
- 1185 Maupin M. A., Kenny J. F., Hutson S. S., Lovelace J. K., Barber N. L., Linsey K. S. (2014)
1186 Estimated use of water in the United States in 2010 Circular, doi: 10.3133/cir1405.
- 1187 McAuley S. D., Barringer J. L., Paulachok G. N., Clark J. S., Zapecza O. S. (2001) Groundwater
1188 flow and quality in the Atlantic City 800 foot Sand, New Jersey, Geological Survey Report
1189 GSR 41, Trenton, NJ, doi: 10.7282/T38913ZV.
- 1190 Meisler H., Leahy P. P., Knobel L. L. (1984) Effect of eustatic sea-level changes on saltwater-
1191 freshwater in the northern Atlantic Coastal Plain, US Geological Survey Water-Supply
1192 Paper 2255, Alexandria, VA.
- 1193 Menke H. P., Maes J., Geiger S. (2021) Upscaling the porosity-permeability relationship of a
1194 microporous carbonate for Darcy-scale flow with machine learning, Scientific Reports
1195 11(1):2625, doi: 10.1038/s41598-021-82029-2
- 1196 Micallef A., Person M., Berndt C., Bertoni C., Cohen D., Dugan B., Evans R., Haroon A. et al.
1197 (2020a) Offshore freshened groundwater in continental margins, Reviews of Geophysics,
1198 doi: 10.1029/2020RG000706.
- 1199 Micallef A., Person M., Haroon A., Weymer B. A., Jegen M., Schwalenberg K., Faghih Z., Duan
1200 S. et al. (2020b) 3D characterisation and quantification of an offshore freshened
1201 groundwater system in the Canterbury Bight, Nature Communications 11(1):1372, doi:
1202 10.1038/s41467-020-14770-7.
- 1203 Miller K. G., Browning J. V., Mountain G. S., Bassetti M. A., Monteverde D., Katz M. E., Inwood
1204 J., Lofi J. et al. (2013) Sequence boundaries are impedance contrasts: Core-seismic-log
1205 integration of Oligocene-Miocene sequences, New Jersey shallow shelf, Geosphere
1206 9(5):1257–1285.

- 1207 Miller K. G., Snyder S. W. (1997) Island Beach, Atlantic City, and Cape May Sites, New Jersey
1208 Coastal Plain, Proceedings of the Ocean Drilling Program, Scientific Results, 150X,
1209 College Station, TX (Ocean Drilling Program), doi: 10.2973/odp.proc.ir.150X.1994.
- 1210 Miller K. G., Sugarman P., van Fossen M., Liu C., Browning J. V., Queen D., Aubry M.-P.,
1211 Burckle L. D. et al. (1994) Island Beach Site Report. In: Miller KG et al.(eds) Proc. ODP,
1212 Init. Rpts., 150X, College Station, TX (Ocean Drilling Program), doi:
1213 10.2973/odp.proc.ir.150x.111.1994.
- 1214 Monteverde D. H., Mountain G. S., Miller K. G. (2008) Early Miocene sequence development
1215 across the New Jersey margin, *Basin Research* 20(2):249–267.
- 1216 Mook W., Rozanski K. (2000) Environmental isotopes in the hydrological cycle, IAEA Publish
1217 39.
- 1218 Morgan A. V., Ruddiman W. F., Wright H. E. (1987) Late Wisconsin and early Holocene
1219 paleoenvironments of east-central North America based on assemblages of fossil
1220 Coleoptera, *The Geology of North America* 3:353–370.
- 1221 Mountain G., Proust J. N., McInroy D., Cotterill C., Expedition 313 Scientists (2010) Proc. IODP,
1222 313. Integrated Ocean Drilling Program Management International, Inc., Tokyo, doi:
1223 10.2204/iodp.proc.313.2010.
- 1224 O.S.P.O. (2013) Sea Surface Temperature Contour Charts (NOAA Office of Satellite and Product
1225 Operations), <https://www.ospo.noaa.gov/Products/ocean/sst/contour/>, checked on
1226 1/2/2018.
- 1227 Paldor A., Aharonov E., Katz O. (2020) Thermo-haline circulations in subsea confined aquifers
1228 produce saline, steady-state deep submarine groundwater discharge, *Journal of Hydrology*
1229 580:124276, doi: 10.1016/j.jhydrol.2019.124276.
- 1230 Person M., Dugan B., Swenson J. B., Urbano L., Stott C., Taylor J., Willett M. (2003) Pleistocene
1231 hydrogeology of the Atlantic continental shelf, New England, *Geological Society of*
1232 *America Bulletin* 115(11):1324–1343.

- 1233 Pope DA, Gordon AD (1999) Simulation of Ground-water Flow and Movement of the Freshwater-
1234 saltwater Interface in the New Jersey Coastal Plain. U.S. Department of the Interior, U.S.
1235 Geological Survey.
- 1236 Post V. E., Groen J., Kooi H., Person M., Ge S., Edmunds W. M. (2013) Offshore fresh
1237 groundwater reserves as a global phenomenon, *Nature* 504(7478):71–78.
- 1238 Proust J.-N., Pouderoux H., Ando H., Hesselbo S. P., Hodgson D. M., Lofi J., Rabineau M.,
1239 Sugarman P. J. (2018) Facies architecture of Miocene subaqueous clinothems of the New
1240 Jersey passive margin: Results from IODP-ICDP Expedition 313, *Geosphere* 14(4).
- 1241 Ramires M. L., Nieto de Castro C. A., Nagasaka Y., Nagashima A., Assael M. J., Wakeham W.
1242 A. (1995) Standard Reference Data for the Thermal Conductivity of Water, *Journal of*
1243 *Physical and Chemical Reference Data* 24(3):1377–1381, doi: 10.1063/1.555963.
- 1244 Rath V., Wolf A., Bücker H. M. (2006) Joint three-dimensional inversion of coupled groundwater
1245 flow and heat transfer based on automatic differentiation: sensitivity calculation,
1246 verification, and synthetic examples, *Geophysical Journal International* 167(1):453–466.
- 1247 Reynolds A. D. (1999) Dimensions of Paralic Sandstone Bodies, *AAPG Bulletin* 83
1248 (1999)(2):211–229, doi: 10.1306/00AA9A48-1730-11D7-8645000102C1865D.
- 1249 Riedel M., Reiche S., Aßhoff K., Buske S. (2018) Seismic depth imaging of sequence boundaries
1250 beneath the New Jersey shelf, *Marine Geophysical Research*:1–16, doi: 10.1007/s11001-
1251 018-9360-9.
- 1252 Rubin H., Roth C. (1979) On the growth of instabilities in groundwater due to temperature and
1253 salinity gradients, *Advances in Water Resources* 2:69–76, doi: 10.1016/0309-
1254 1708(79)90013-7.
- 1255 Ryan W. B., Carbotte S. M., Coplan J. O., O'Hara S., Melkonian A., Arko R., Weissel R. A.,
1256 Ferrini V. et al. (2009) Global Multi-Resolution Topography synthesis, *Geochemistry,*
1257 *Geophysics, Geosystems* 10(3):n/a-n/a, doi: 10.1029/2008GC002332.

- 1258 Seifert D., Jensen J. L. (1999) Using sequential indicator simulation as a tool in reservoir
1259 description: issues and uncertainties, *Mathematical Geology* 31(5):527–550.
- 1260 Selley, RC, Sonnenberg, SA (eds.) (2015) *Elements of petroleum geology*. Third edition. Elsevier
1261 Academic Press is an imprint of Elsevier, Amsterdam, Boston.
- 1262 Siegel D. I. (1991) Evidence for dilution of deep, confined ground water by vertical recharge of
1263 isotopically heavy Pleistocene water, *Geology* 19(5):433, doi: 10.1130/0091-
1264 7613(1991)019<0433:EFDODC>2.3.CO;2.
- 1265 Siegel J., Person M., Dugan B., Cohen D., Lizarralde D., Gable C. (2014) Influence of late
1266 Pleistocene glaciations on the hydrogeology of the continental shelf offshore
1267 Massachusetts, USA, *Geochemistry, Geophysics, Geosystems* 15(12):4651–4670, doi:
1268 10.1002/2014GC005569.
- 1269 Simmons C. T., Fenstemaker T. R., Sharp J. M. (2001) Variable-density groundwater flow and
1270 solute transport in heterogeneous porous media: approaches, resolutions and future
1271 challenges, *Journal of Contaminant Hydrology* 52(1-4):245–275, doi: 10.1016/S0169-
1272 7722(01)00160-7.
- 1273 Szymkiewicz A. (2013) Upscaling from Darcy Scale to Field Scale. In A Szymkiewicz
1274 (ed.) *Modelling Water Flow in Unsaturated Porous Media*. Springer Berlin Heidelberg,
1275 Berlin, Heidelberg:139–175.
- 1276 Thomas A. T., Reiche S., Riedel M., Clauser C. (2019) The fate of submarine fresh groundwater
1277 reservoirs at the New Jersey shelf, USA, *Hydrogeology Journal*, doi: 10.1007/s10040-019-
1278 01997-y.
- 1279 Vajdova V., Baud P., Wong T.-f. (2004) Permeability evolution during localized deformation in
1280 Bentheim sandstone, *Journal of Geophysical Research* 109(B10), doi:
1281 10.1029/2003JB002942.
- 1282 Varma S., Michael K. (2012) Impact of multi-purpose aquifer utilisation on a variable-density
1283 groundwater flow system in the Gippsland Basin, Australia, *Hydrogeology Journal*
1284 20(1):119–134.

1285 van Geldern R., Hayashi T., Böttcher M. E., Mottl M. J., Barth J. A., Stadler S. (2013) Stable
1286 isotope geochemistry of pore waters and marine sediments from the New Jersey shelf:
1287 Methane formation and fluid origin, *Geosphere* 9(1):96–112.

1288 Wagner F. M., Uhlemann S. (2021) Chapter One - An overview of multimethod imaging
1289 approaches in environmental geophysics. In Cedric Schmelzbach (ed.) *Inversion of*
1290 *Geophysical Data*. *Advances in Geophysics*, vol. 62. Elsevier, The Netherlands:1–72.

1291 Zamrsky D., Karssenberg M. E., Cohen K. M., Bierkens M. F., Oude Essink G. H. (2020)
1292 Geological Heterogeneity of Coastal Unconsolidated Groundwater Systems Worldwide and Its
1293 Influence on Offshore Fresh Groundwater Occurrence, *Frontiers in Earth Science* 7:2844, doi:
1294 10.3389/feart.2019.00339.

1295